frontiers in Marine Science

ORIGINAL RESEARCH
published: 30 September 2019
doi: 10.3389/fmars.2019.00591

Shelf Inputs and Lateral Transport of Mn, Co, and Ce in the Western North Pacific Ocean

Peter L. Morton[1], William M. Landing[2], Alan M. Shiller[3], Amy Moody[3], Thomas D. Kelly[2], Michael Bizimis[4], John R. Donat[5], Eric H. De Carlo[6] and Joseph Shacat[7]*

[1] National High Magnetic Field Laboratory, Tallahassee, FL, United States, [2] Earth, Ocean, and Atmospheric Science, Florida State University, Tallahassee, FL, United States, [3] Division of Marine Science, University of Southern Mississippi, Hattiesburg, MS, United States, [4] School of the Earth, Ocean and Environment, University of South Carolina, Columbia, SC, United States, [5] Department of Chemistry and Biochemistry, Old Dominion University, Norfolk, VA, United States, [6] Department of Oceanography, University of Hawai'i at Mānoa, Honolulu, HI, United States, [7] National Asphalt Pavement Association, Annapolis, MD, United States

OPEN ACCESS

Edited by:
Johan Schijf, Chesapeake Biological Laboratory, University of Maryland Center for Environmental Science (UMCES), United States

Reviewed by:
Hein De Baar, Royal Netherlands Institute for Sea Research (NIOZ), Netherlands
Antonio Cobelo-Garcia, Spanish National Research Council (CSIC), Spain

***Correspondence:**
Peter L. Morton
pmorton@fsu.edu

Specialty section:
This article was submitted to Marine Biogeochemistry, a section of the journal Frontiers in Marine Science

Received: *28 February 2019*
Accepted: *05 September 2019*
Published: *30 September 2019*

Citation:
Morton PL, Landing WM, Shiller AM, Moody A, Kelly TD, Bizimis M, Donat JR, De Carlo EH and Shacat J (2019) Shelf Inputs and Lateral Transport of Mn, Co, and Ce in the Western North Pacific Ocean. Front. Mar. Sci. 6:591. doi: 10.3389/fmars.2019.00591

The margin of the western North Pacific Ocean releases redox-active elements like Mn, Co, and Ce into the water column to undergo further transformation through oxide formation, scavenging, and reductive dissolution. Near the margin, the upper ocean waters enriched in these elements are characterized by high dissolved oxygen, low salinity, and low temperature, and are a source of the North Pacific Intermediate Water. High dissolved concentrations are observed across the Western Subarctic Gyre, with a rapid decrease in concentrations away from the margin and across the subarctic-subtropical front. The particulate concentrations of Mn, Co, and Ce are also high in the subarctic surface ocean and enriched relative to Ti and trivalent rare earth elements. Furthermore, the particles enriched in Mn, Co, and Ce coincide at the same depth range, suggesting that these elemental cycles are coupled through microbial oxidation in the subarctic gyre as the waters travel along the margin before being subducted at the subarctic-subtropical front. Away from the margin, the Mn, Co, and Ce cycles decouple, as Mn and Ce settle out as particles while dissolved Co is preserved and transported within the North Pacific Intermediate Water into the central North Pacific Ocean.

Keywords: oxygen minimum zone (OMZ), biogeochemistry, North Pacific Intermediate Water (NPIW), western subarctic North Pacific, mixed water region between Kuroshio and Oyashio, manganese, cobalt, cerium anomaly

INTRODUCTION

The lateral transport of material from continental margins can provide essential trace metals to the ocean (Westerlund et al., 1986; Elrod et al., 2004; Lam et al., 2006; Lam and Bishop, 2008; Aguilar-Islas et al., 2013; Noble et al., 2017; Tagliabue et al., 2017). While surface maxima of manganese (Mn) may result from atmospheric deposition or freshwater inputs (Shiller, 1997; van Hulten et al., 2016), numerous studies have established the importance of Mn as a tracer of redox mobilized sediment inputs from continental margins in the upper ocean. Dissolved Mn (dMn) is released from sediments during reductive dissolution driven by bacterial respiration of organic matter and associated diagenetic processes (Sundby et al., 1986; Burdige, 1993, 2006). Fluxes of dMn can persist across the sediment-water interface even when overlying waters are suboxic or oxic and produce a

characteristic subsurface plume enriched in dissolved Mn (Landing and Bruland, 1980; Bishop and Fleisher, 1987; Stumm and Morgan, 1995; Minakawa et al., 1996; Chase et al., 2005; Vedamati et al., 2015; Oldham et al., 2017).

Manganese-enriched plumes (both dissolved and particulate) have been observed along the coastlines of major ocean basins, including Tokyo Bay (Noriki et al., 1997); the Japan Trench (Otosaka and Noriki, 2000); the North Pacific Ocean (e.g., Martin et al., 1985); the Peru margin (Vedamati et al., 2015); the Arctic Ocean (Aguilar-Islas et al., 2007; Middag et al., 2011b); the Southern Ocean in general (Middag et al., 2011a; Sherrell et al., 2018), especially along the Antarctic Peninsula into the Weddell Sea (Middag et al., 2013) and across the Drake Passage (Middag et al., 2012; Klunder et al., 2014); the Indian Ocean (Saager et al., 1989; Lewis and Luther, 2000; Vu and Sohrin, 2013); the eastern North Atlantic Ocean (Tachikawa et al., 1999); the South Atlantic Ocean at the Benguela/Angola front (Noble et al., 2012); and the Kuril-Kamchatka margin (Lam and Bishop, 2008; Lamborg et al., 2008).

In addition to Mn, other trace elements can be similarly released from margin sediments via redox mobilization, including Co (Noble et al., 2012, 2017; Hawco et al., 2016; Tagliabue et al., 2018) and Ce (Zhang and Nozaki, 1998; Obata et al., 2007; Zheng et al., 2016). While Co also undergoes similar redox cycling in seawater, both reduced and oxidized forms can exist in the soluble phase (Moffett and Ho, 1996), often through stabilization with organic ligands (Saito and Moffett, 2001; Hawco et al., 2016, 2018; Noble et al., 2017; Tagliabue et al., 2018). In contrast, while the reduced forms of Mn and Ce are generally found in the aqueous phase, the oxidized forms are found in the particulate phase (Stumm and Morgan, 1995; Moffett and Ho, 1996; Nozaki, 2001).

Plumes of dMn can be oxidized in the water column to produce particles enriched in Mn over crustal abundance relative to a non-redox active trace element like Al or Ti (Tanoue and Midorikawa, 1995; Lam and Bishop, 2008; Lamborg et al., 2008; Yiğiterhan et al., 2011; Lam et al., 2015; Oldham et al., 2017). These Mn-enriched particles have been reported with similar enrichments in particulate Co and Ce, leading naturally to conclusions that these elements are oxidized via a similar mechanism such as microbial oxidation (Moffett, 1990, 1994b; Moffett and Ho, 1996; Bargar et al., 2000; Tebo et al., 2004; Murray et al., 2007; Spiro et al., 2010). Similar enrichments (or depletions) in Ce can be identified by the Ce anomaly (Elderfield, 1988), where the actual concentration of dissolved or particulate Ce is compared to the concentration of Ce predicted from its lanthanide neighbors (i.e., La and Pr). While all the REEs will passively adsorb and desorb from other marine suspended particles (to varying degrees), Ce(III) can be oxidized to Ce(IV) and form oxides that remain as particles even when the other REEs desorb from particles and return to the dissolved pool, thus producing the observed Ce anomaly (Equation 1):

$$Ce\ anomaly = \frac{2(CeSN)}{(LaSN + PrSN)} \quad (1)$$

where *CeSN*, *LaSN* and *PrSN* represent the shale-normalized REE concentrations using Post-Archean Australian Shale (PAAS) as in Rudnick and Gao (2003).

The redox activities of Mn, Co, and Ce also depend on other chemical and biological factors. Low oxygen conditions in sediments can release dissolved elements into the overlying water column (Sundby et al., 1986). If this bottom water is also low in oxygen, then the reduced forms may enjoy longer residence times. Photochemical reduction (in reactions with dissolved organic carbon and sunlight) may also prolong the residence time of Mn in seawater (Sunda and Huntsman, 1994). Biological Mn oxidation via bacterial or fungal mediated processes can transform dissolved Mn to particles, and numerous studies have shown that Co and Ce are similarly oxidized by the same enzymatic pathway or by secondary oxidation by the reactive particulate Mn-oxides (Tebo et al., 1984; Moffett, 1990, 1994b, 1997; Moffett and Ho, 1996; De Carlo et al., 1997; Murray et al., 2007; Spiro et al., 2010; Schijf et al., 2015; Toyoda and Tebo, 2016). Although Ce has been shown to oxidize abiotically (De Carlo et al., 1997), studies of Ce oxidation kinetics conducted using seawater suggest a microbial role linked to Mn oxidation and rates that are depth-dependent, where oxidation is photo-inhibited in surface waters but increase with depth (Moffett, 1994a,b). Therefore, particles enriched in Mn, Co, and Ce can at least partly (if not primarily) result from biological processes.

Redox mobilized shelf inputs of dissolved trace elements can be preserved and transported offshore when the overlying waters are also low in oxygen, especially in regions like the northern Indian Ocean, the eastern Atlantic Ocean, and the eastern North and South Pacific Oceans (Breitburg et al., 2018; Scholz, 2018). In the northern Indian Ocean, the depths of the minimum oxygen concentrations coincide with plumes of dissolved trace elements like Mn (Saager et al., 1989; Lewis and Luther, 2000), Fe (Saager et al., 1989; Kondo and Moffett, 2013; Vu and Sohrin, 2013; Grand et al., 2015a,b; Chinni et al., 2019), Co (Vu and Sohrin, 2013), and Ce (German and Elderfield, 1990). In the eastern South Atlantic, during the CoFeMUG cruise (Noble et al., 2012; Zheng et al., 2016), Mn, Co, Fe, and Ce were all enriched in subsurface plumes within the depth range of the oxygen minimum zone. Similar inputs of Fe (Buck et al., 2015; Fitzsimmons et al., 2015a; Hatta et al., 2015; Sedwick et al., 2015; Klar et al., 2018), Mn (Wu et al., 2014; Hatta et al., 2015), and Co (Noble et al., 2017) were found in low oxygen waters along the Mauritanian coast. The oxygen minimum zones of the eastern North and/or South Pacific regions contain high concentrations of dissolved Mn (Vedamati et al., 2015; Chen and Wu, 2019), Fe (Noffke et al., 2012; Chever et al., 2015; Glass et al., 2015; Kondo and Moffett, 2015; Heller et al., 2017; Buck et al., 2018; Cutter et al., 2018; Marsay et al., 2018), Co (Saito et al., 2004; Hawco et al., 2016), and other redox active elements like iodide (Cutter et al., 2018). Similar studies conducted in the Cariaco Basin (Jacobs et al., 1987; de Baar et al., 1988) and the Black Sea (e.g., Lewis and Landing, 1991; Yiğiterhan et al., 2011) show the prevalence of concurrent inputs of redox active metals in a variety of basins. In summary, while marine margin sediments can act as a source of redox active trace elements to the overlying waters, the oxygen minimum zones allow for extended residence times

of soluble reduced elements and lateral transport far beyond the immediate coastline.

In the subtropical and subarctic North Pacific Ocean, the oxygen minimum zone extends across the entire basin from east to west (Paulmier and Ruiz-Pino, 2009), and redox-mobilized shelf inputs of dissolved trace elements have been observed along nearly every coast. Margin inputs have been identified by the lateral transport of dissolved Mn (Landing and Bruland, 1980, 1987; Martin et al., 1985; Johnson et al., 1996; Chase et al., 2005; Noble et al., 2008), Fe (Boyle et al., 2005; Chase et al., 2005; Elrod et al., 2004; Noble et al., 2008; Fitzsimmons et al., 2015b), Co (Knauer et al., 1982; Fujishima et al., 2001; Ezoe et al., 2004; Noble et al., 2008), and Ce (de Baar et al., 1985; de Baar et al., 2018). Lateral inputs of particulate Mn and Fe (Lam and Bishop, 2008; Lamborg et al., 2008) were also found in subsurface waters within the oxycline above the low-oxygen waters, but observations in the western North Pacific were limited to a single station (time-series Station K2) so the extent of offshore transport remained undetermined. Nishioka et al. (2007) suggested that material in the western North Pacific could be swept even further into the open ocean by currents circulating in this region. A recent study of three Japanese GEOTRACES cruises established the importance of margin inputs and basin-wide intermediate water masses in the distributions of dissolved Mn and Co (Zheng et al., 2019).

The ocean currents provide boundaries and drive the major features of the North Pacific Ocean. The Western Subarctic Gyre (WSG) is formed by the southward moving East Kamchatka Current along the Kuril-Kamchatka margin, the Alaskan Stream to the north along the Aleutian Islands, and the Kuroshio Current and Extension to the south. This circulation drives upwelling in the WSG, which brings nutrient-rich intermediate waters to the surface and creates a high nutrient-low chlorophyll (HNLC) regime (Brown et al., 2005; Kinugasa et al., 2005; Nishioka et al., 2007; Misumi et al., 2011; Tanaka et al., 2012). The long-distance transport of crustal material from the Kuril-Kamchatka and Aleutian Margins can supply much-needed Fe to the western North Pacific (Brown et al., 2005; Measures et al., 2005; Nishioka et al., 2007; Hsu et al., 2008; Okin et al., 2011; Tanaka et al., 2012; Okubo et al., 2013; Takeda et al., 2014), which remains Fe-limited despite predictions of aerosol fluxes from Asian deserts and industry (Jickells et al., 2005; Mahowald et al., 2005, 2009).

The 2002 Intergovernmental Oceanographic Commission (IOC-2002) expedition was conducted in April-May 2002 and included three vertical profile stations along the western North Pacific margin including Station KNOT (44°N 150°E) as well as six other vertical profile stations and daily surface water collections extending from Japan to Hawaii in the central North Pacific (**Figure 1**). By analyzing water samples at the three margin stations for dissolved and particulate Mn, Co, and Ce, we demonstrate sedimentary inputs along the entire Kuril-Kamchatka margin. While our research does not directly address biological processes, our evidence suggests that microbial oxidation is partly responsible for converting the dissolved sedimentary inputs to enriched particles which increase in concentration in water masses flowing along the margin. These currents are identified according to their temperature/salinity signatures, potential densities, and oxygen content, and will be shown to carry some portion of the shelf-derived material into the central North Pacific. Particle settling removes most Mn and Ce, but Co is preserved in the dissolved phase and incorporated into the North Pacific Intermediate Water, observed as far away as Hawaii. Here, using dissolved and particulate concentrations of Mn, Co, Ce and other contextual elements, the spread of redox-mobilized shelf material is shown to be varyingly influenced by microbial oxidation, energetic frontal subduction, and long-range lateral transport.

MATERIALS AND METHODS

Surface Sampling

Seawater was pumped through a towed surface-sampler package ("Fish") that was deployed at about 0.5 m depth while the *R/V Melville* was underway (Measures et al., 2006). The seawater was pumped to a HEPA-filtered laminar flow bench through acid-washed Teflon tubing. Dissolved metal samples were collected after the seawater passed through a 0.2-μm Gelman Criti–cap polysulfone cartridge filter into acid-washed 1 L HDPE bottles. Samples were acidified (∼pH 1.7; 0.024 M), using 2 mL of concentrated ultrapure HCl (Fisher, Optima grade) per 1 L of sample. The samples were stored acidified for at least 6 months before analysis to ensure complete release of metals from any organic complexes.

Vertical Profile Sampling

Vertical profile samples of dissolved and particulate trace elements were collected using 30-L Teflon-coated Go-Flo bottles (General Oceanics) hung on a Kevlar line and lowered to pre-determined depths at nine stations. After the bottles were tripped and recovered, they were moved inside one of the ship's bays that had been converted into a positive-pressure clean lab supplied with HEPA-filtered air. Subsamples were drawn from the Go-Flo bottles by pressurizing them with filtered compressed air (∼0.5 atm overpressure), forcing the seawater through an acid-washed (1.2 M HCl) 0.4-μm pore size, 142-mm diameter polycarbonate track-etched (PCTE) Nuclepore filter. Dissolved samples were collected in acid-washed 1 L HDPE bottles and acidified like the surface samples. The Nuclepore filters were folded into quarters to contain all particulate material on the inside of the filter and placed in plastic zip-lock bags. Particulate samples were immediately frozen and kept frozen until digestion and analysis.

Dissolved Sample Analysis

Filtered seawater samples were collected for dissolved trace metals and the rare earth element suite. As this paper presents the cycling of Mn, Co, and Ce, only these elements and those supporting their focused interpretation (e.g., La and Pr) are included here. However, additional manuscripts are currently in preparation that will describe the bioactive trace metals (e.g., Fe, Cd) and the extended REE series.

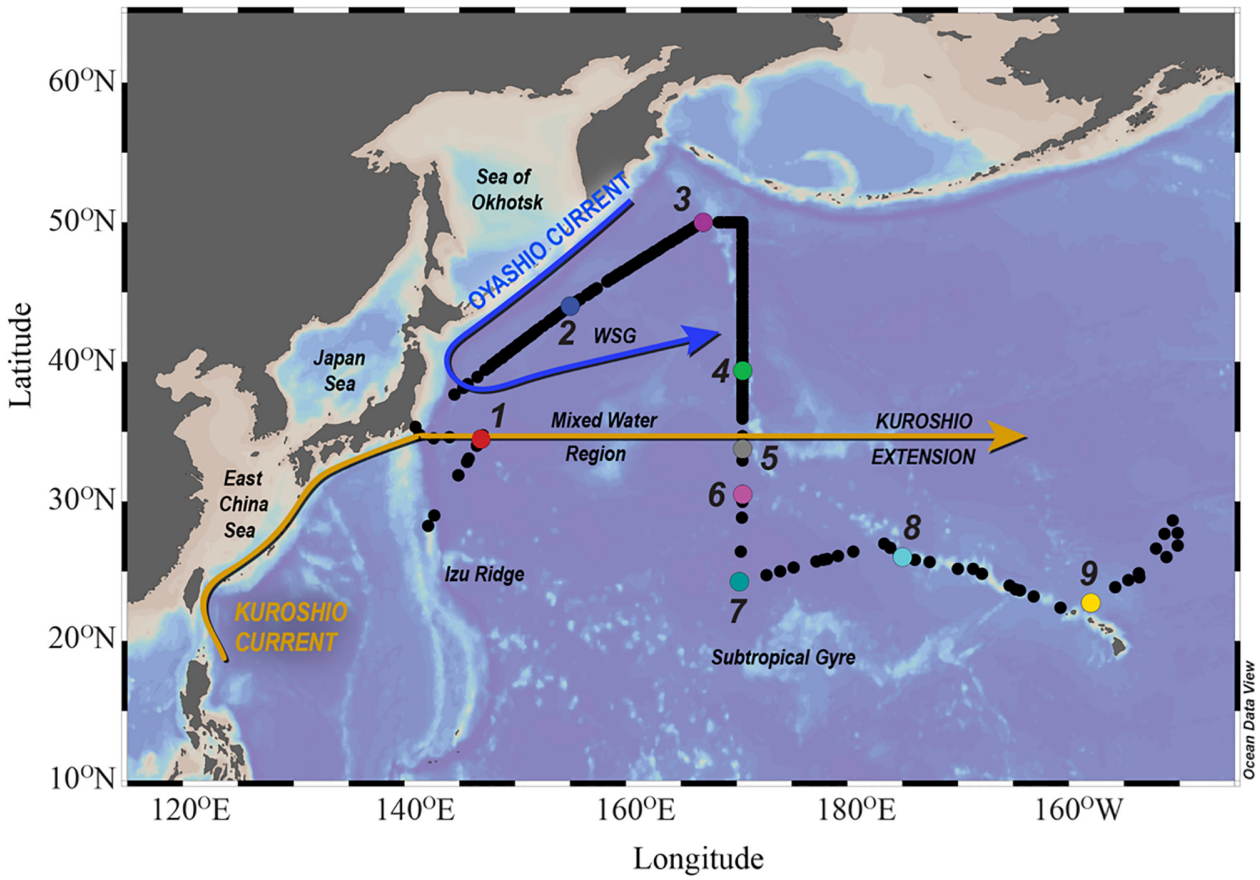

FIGURE 1 | Map of the IOC-2002 study region: Map of the IOC-2002 study region, including relevant regions and currents. WSG, Western Subarctic Gyre. Black dots indicate surface sampling stations, while colored dots indicate vertical profile stations. Station colors are consistent throughout the figures.

Dissolved Trace Metals

Dissolved Mn and Co were extracted in 2007–2008 (FSU) from seawater using an 8-hydroxyquinoline (8HQ) resin column according to Milne et al. (2010). In brief, 60 mL aliquots of sample (acidified to pH 1.7) were UV oxidized for 1 h (Hg-vapor lamp, 1200 W). After allowing the UV-treated samples to cool, 12 mL aliquots of each were poured into acid-washed 15-mL polypropylene centrifuge tubes. To quantify the concentrations of dissolved Mn and Co, a series of standard additions (n = 4) were made every 6–10 samples, and the samples allowed to equilibrate overnight. Fifteen minutes before extraction onto the 8HQ resin column, each individual aliquot was pH adjusted and buffered using a 2 M ammonium-acetate solution to a final pH of 5.5–6.0 (∼0.17 M acetate, or ∼1 mL buffer solution per 12 mL acidified seawater sample). Once the trace metals in the samples were loaded onto the column (2 mL/min flow rate), the column was rinsed with ultrapure water and the analyte metals were eluted with 1 mL of 1.5 M quartz distilled HNO_3 and analyzed using an ELEMENT ICP-MS in medium resolution (National High Magnetic Field Laboratory, Tallahassee, FL, United States). Dissolved concentrations of Mn and Co were measured in the SAFe S and D2 consensus reference materials and were contributed to the original intercalibration study (**Supplementary Table 1**). Dissolved Mn concentrations for SAFe S and D2 were determined to be 0.90 ± 0.06 nM (vs. the consensus value of 0.79 ± 0.06 nM) and 0.46 ± 0.05 nM (vs. 0.35 ± 0.05 nM), respectively. Concentrations of dissolved Co in the SAFe D2 samples (40.5 ± 1.7 pM) were close to the consensus value (45.7 ± 2.9 pM) while our dCo measurements of the SAFe S sample were lower than the consensus value (2.2 ± 1.5 pM vs. 4.8 ± 1.2 pM) despite our use of UV oxidation prior to extraction. There is still much uncertainty over the UV intensity and duration required to release dCo from natural organic ligands. Only six labs have reported dCo in the SAFe S samples following UV oxidation, with reported concentrations ranging from 2 to 7 pM (close to the reported detection limits). Because of this uncertainty, we did not make any yield corrections to our dCo data, but this does not affect our interpretation of the dCo distributions and the processes affecting dCo in our study region. Comparisons of dMn and dCo with other studies conducted near the Hawaiian islands are shown in **Figure 2**.

Dissolved Rare Earth Elements (REEs)

Another set of concurrently collected samples were analyzed in 2016-2017 (USM) for dissolved La, Ce, and Pr, as part of the entire suite of rare earth elements. A 14-mL aliquot of sample

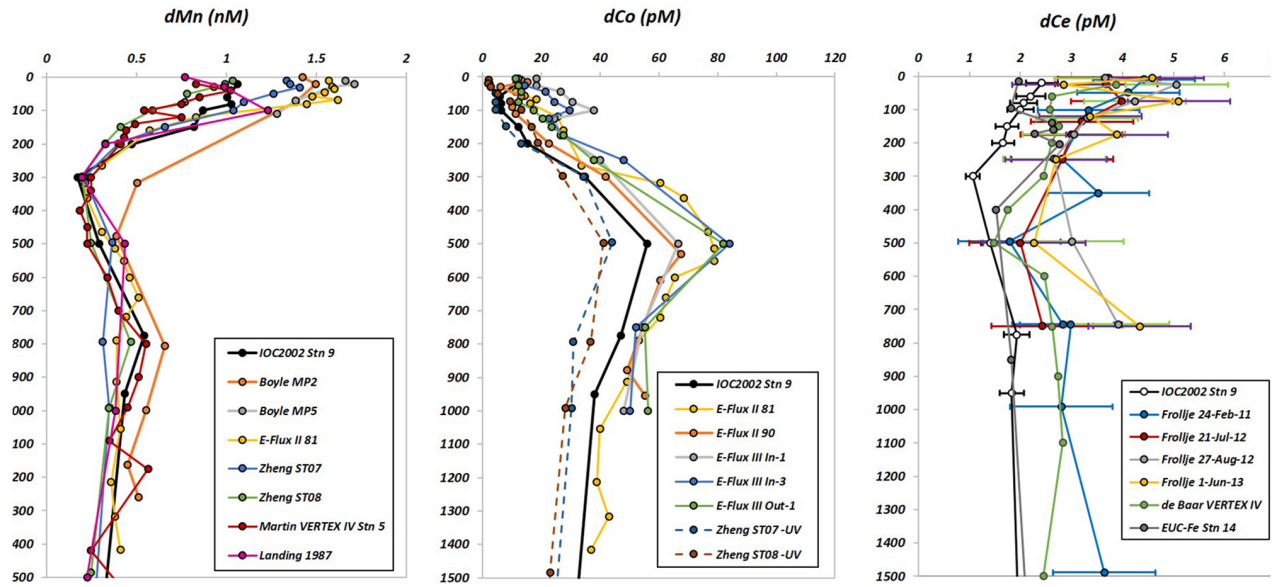

FIGURE 2 | Comparison of vertical profiles of dissolved Mn **(left)**, Co **(center)**, and Ce **(right)**. Error bars (±1 σ) are shown for Ce. **dMn - IOC2002 Stn 9** = this study, **Boyle MP2** = station ALOHA, 26 April 2001 (Boyle et al., 2005), **Boyle MP5** = station ALOHA, 1 July 2002 (Boyle et al., 2005), **E-Flux II 81** = 20.27°N, 156.94°W (Noble et al., 2008), **Zheng ST07** = 20.001°N, 160.002°W (Zheng et al., 2019), **Zheng ST08** = 26.33°N, 160.002°W (Zheng et al., 2019), **Martin VERTEX IV Stn 5** = 28.0°N, 155.0°W (Martin et al., 1985), **Landing 1987** = 14.7°N, 160°W (Landing and Bruland, 1987). **dCo - IOC2002 Stn 9** = this study, **E-Flux II 81** = 20.27°N, 156.94°W (Noble et al., 2008), **E-Flux II 90** = 20.50°N, 157.50°W (Noble et al., 2008), **E-Flux III In-1** = 19.36°N, 157.08°W (Noble et al., 2008), **E-Flux In-3** = 19.12°N, 157.03°W (Noble et al., 2008), **E-Flux III Out-1** = 20.62°N, 157.59°W (Noble et al., 2008), **Zheng ST07 -UV** = 20.001°N, 160.002°W, without UV oxidation (Zheng et al., 2019), **Zheng ST08 -UV** = 26.33°N, 160.002°W, without UV oxidation (Zheng et al., 2019). **dCe - IOC2002 Stn 9** = this study, **Frollje 24-February-11** = station ALOHA (Frollje et al., 2016), **Frollje 21-July-12** = station ALOHA (Frollje et al., 2016), **Frollje 27-Aug-12** = station ALOHA (Frollje et al., 2016), **Frollje 1-June-13** = station ALOHA (Frollje et al., 2016), **de Baar VERTEX IV** = 28°N 155°W, 14 July 1983 (de Baar et al., 2018), **EUC-Fe Stn 14** = 0°N 180°W, 10 September 2006 (Grenier et al., 2013).

was spiked with a mixture of isotopically enriched Nd-145, Sm-149, Eu-153, Gd-155, Dy-161, Er-167, and Yb-171 (Oak Ridge National Laboratories). Each spike was >90% enriched in the listed isotopes. The sample/spike ratio was optimized so that the analytical isotope ratios fall at the geometric mean of the natural and enriched spike isotope ratios, thereby minimizing error. Samples were then extracted/pre-concentrated using a SeaFAST system (Elemental Scientific, Inc.) operated in offline mode, similar to the method described by Hathorne et al. (2012). The extracted samples were subsequently analyzed using a Thermo-Fisher ELEMENT XR ICP-MS operated in low-resolution mode with an Apex-FAST high efficiency sample introduction system with Spiro desolvator (Elemental Scientific, Inc.). The enriched isotope spikes also served to provide counts/second calibration factors for elements that were not spiked with enriched isotopes. This calibration was also examined with a mixed REE standard made in dilute 0.16 M HNO_3. Precision and recovery were checked by analysis of a large-volume composite North Atlantic surface seawater sample. Spiked (with a natural isotopic abundance elemental spike) and unspiked aliquots of this sample were analyzed twice in each analytical run. Concentrations of La, Ce, and Pr in samples collected at the Bermuda Atlantic Time Series location during the 2011 U.S. GEOTRACES North Atlantic expedition compared favorably with published concentrations (Pahnke et al., 2012; van de Flierdt et al., 2012; Middag et al., 2015) and revealed no significant low REE oxide interferences on middle and heavy REEs. A detailed report of this intercomparison exercise is included as **Supplementary Document 1**, and the comparison of dCe concentrations with those of other studies conducted near Hawaii is shown in **Figure 2**.

Particulate Sample Analysis

To determine the lithogenic, biogenic, and authigenic fractions in the particulate samples, a total digestion method was employed (FSU, 2008), modified from the Eggimann and Betzer (1976) procedure and later thoroughly tested in Ohnemus et al. (2014). In brief, 2 mL of an acid mixture containing 4 M each of HNO_3 (quartz distilled), HCl (Fisher Optima), and HF (Teflon distilled) was added to a 15-mL Teflon jar (Savillex) to submerge a folded 142 mm PCTE filter. The jars were sealed and placed on an enclosed HEPA-filtered laminar flow hotplate ("flowbox") for 3 h at 100–120°C. The jars were removed from the heat and allowed to cool before removing the lids in a fume hood. Using a Teflon spatula and tweezers, each folded filter was removed from the solution and all possible liquid was squeezed into the digestion jar. The filter was then twice rinsed with ultrahigh purity water (18.2 MOhm-cm), squeezing after each rinse. Once all the filters had been rinsed and removed, the jars were returned to the hotplate where they were heated at 120°C until taken to dryness, usually overnight. To oxidize any remaining organic material, 2 mL of 7M HNO_3 (quartz distilled) was added to the residue and the open jars were returned to the hotplate at 100-120°C until

the samples were once again taken to dryness. Finally, the digest residue was dissolved and transferred to an acid-washed plastic vial using repeated rinses of 0.32 M HNO_3 (∼2%, quartz distilled) up to 20 mL final volume. Concentrations were determined using a multi-element standard in 2% HNO_3 (High Purity Standards) with 1 ppb In correction, and validated against similarly digested samples of the USGS CRM RGM-1, using values reported by Eggins et al. (1997) and the Max-Planck Institute database of Geological and Environmental Reference Materials (GeoReM, 2009). Subsequent testing of this method was shown to yield acceptable recoveries for other reference materials such as NRC PACS-2 and BCR-414 (**Supplementary Table 1**; Ohnemus et al., 2014). The procedural sample precision was determined from replicate analyses of the PACS-2 (n = 5) and BCR-414 reference materials (n = 10) to be 3–5% and 3–4%, respectively, for all elements presented here.

Hydrographic Parameters and Nutrient Analyses

Temperature, salinity, and dissolved oxygen were determined shipboard on samples collected from the ship's rosette and from *in situ* measurements made by the Seabird 911 + CTD (Measures et al., 2006). Since the original publication of the nitrate, phosphate, and silicate data (Measures et al., 2006), it was determined that the nutrient sample storage and analyses were not performed to contemporary standards, so nutrient concentrations discussed here are for qualitative purposes only.

RESULTS

The North Pacific Ocean can be divided into three general hydrographic regions (**Figure 1**): the Western Subarctic Gyre (WSG) in the north (stations 2 and 3), the Subtropical Gyre (STG) in the south (stations 7–9), and the Mixed Water Region (MWR) between the two gyres (stations 1 and 4–6). The results presented here begin with an introduction of the general hydrography of each region with additional attention given to specific relevant hydrographic features, followed by a summary of the distributions of the dissolved and particulate elemental concentrations.

Surface Distributions of Dissolved Trace Elements

The WSG is an upwelling region, characterized by low temperatures (3-4°C), low salinities (32.5–33.1), and high dissolved oxygen concentrations (∼320 μM; **Figure 3**). Consistent with the upwelling characterization, the surface waters contain high dissolved trace element concentrations (**Figure 4**). Surface concentrations (0–10 m depth) of dissolved Mn, Co, La, and Ce (as well as Pr, not shown) were highest in the upwelling WSG (**Figure 4**), following the same general distribution of low temperature and salinity values. Concentrations of dMn averaged 1.25 ± 0.52 nM (range: 0.80–3.26 nM), and concentrations of dCo averaged 23.5 ± 31.4 pM (range: 0.4–86.8 pM). The highest dissolved concentrations of both metals in the WSG were found near the outflow of the Sea of Okhotsk near station 2, and dissolved concentrations were lowest across the STG. Similarly, the average concentrations of the dREEs La (8.0 ± 8.9–pM), Ce (3.7 ± 2.7 pM), and Pr (1.7 ± 1.3 pM) were also highest in the WSG and lowest in the STG and exhibited narrower concentration ranges over the study region than did the other metals.

Vertical Distributions of Dissolved and Particulate Trace Elements

Western Subarctic Gyre (WSG): Stations 2 (KNOT; 44°N, 150°E) and 3 (50°N, 167°E)

The surface properties of the WSG extend through the winter (0–60 m) and spring mixed layers (60–150 m; **Figure 5**) and the vertical profiles of dissolved trace elements follow similar patterns (**Figure 6**). The dMn concentrations were highest (1.7–2.1 nM) in the upper 300 m in the WSG stations 2 and 3, but exhibited dual maxima at both stations: the shallower maximum occurring at 60 m and the deeper maximum occurring at 300 m, with a localized minimum (1.2–1.3 nM) centered at 100–150 m. In contrast, dCo exhibited only a single surface maximum (85–103 pM) at both stations, with the maximum at station 2 more pronounced (centered at 100 m) than the broader maximum (0–300 m) observed at station 3. The vertical profiles of the REEs dLa and dPr steadily increased from the surface (dLa 21–24 pM, dPr 3–3.6 pM) to 1500 m (dLa 44–46 pM, dPr 5–5.6 pM; **Supplementary Table 2**). In contrast, a dCe maximum was observed in the upper 100 m at station 2 (11 pM) and a less pronounced dCe maximum (5 pM) observed in the upper 100 m at station 3. Below 100 m, the dCe concentrations remained between 2 and 4 pM down to 1500 m.

While the vertical distributions of dissolved trace element concentrations were similar between the WSG stations 2 and 3, the particulate concentrations differed greatly (**Figure 7**). At station 2, particulate concentrations of Mn, Co, and Ce were highest in the upper 300 m, with maxima occurring at 100–200 m. The pMn maximum was broader (0.43–0.45 nM at 80–150 m) than that of pCe (2.1 pM at 80 m), and pCo exhibited a dual-maximum feature (3.3 pM at 60 m, 3.5 pM at 150 m). Below these maxima, the concentrations decreased rapidly except for a local maximum at 900 m for pMn, pCo, and pCe (0.17 nM, 2.0 pM, and 1.1 pM, respectively).

At station 3, the pMn concentrations were lower than at station 2, with concentrations increasing from 0.03 nM at 24 m to ∼0.10 nM at 153–300 m, and remaining at 0.09–0.13 nM from 500–1500 m. Concentrations of pLa (0.29–0.92 pM) and pPr (0.03–0.09 pM) exhibited maxima at 63–103 m, while pCe (0.32–0.78 pM) increased from the surface to 1500 m and showed a smaller maximum coinciding with those of pLa and pPr at 103 m. In general, pCo concentrations remained steady through the upper 1500 m at values near 1 pM (0.7–1.5 pM) except for a sharp maximum at 83 m.

Kuroshio Current/Mixed Water Region: Station 1 (34.5°N, 147°E)

At station 1, located within the MWR just off the coast of Japan (**Figure 1**), multiple water masses converge to form different

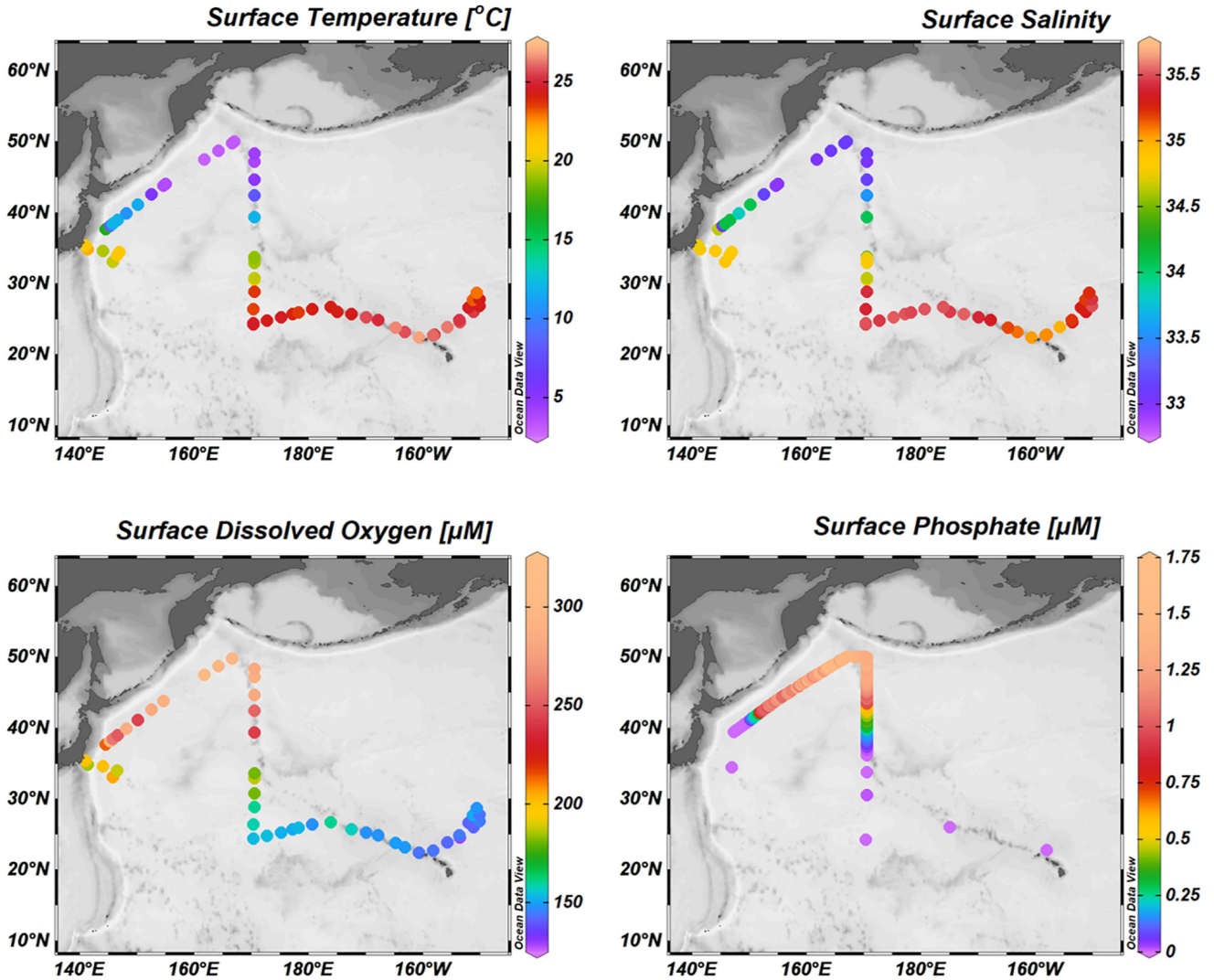

FIGURE 3 | Surface distributions of physical and chemical parameters: the surface distributions of temperature, salinity, dissolved oxygen, and major nutrients like phosphate reflect the physical circulation of the North Pacific Ocean (Measures et al., 2006). The upwelling waters of the western subarctic gyre are characterized by low temperatures and salinities but high concentrations of dissolved oxygen and phosphate. In contrast, the downwelling subtropical gyre is characterized by higher temperatures and salinities but lower concentrations of dissolved oxygen and nearly undetectable concentrations of phosphate.

layers, distinguishable by their physical and chemical properties (**Figure 8**). Below the surface waters of the Kuroshio Current (0–300 m, 24.5–26.6 σ_θ), a low temperature-low salinity intrusion can be seen at 455 m (**Figure 5**) coinciding with σ_θ = 26.4 (**Figure 8**). A second low temperature/low salinity intrusion is also seen at 647 m (26.9 σ_θ), interwoven with the lower portion of the Kuroshio Current (527 m, 26.6 σ_θ; **Figure 8**).

The water mass observed at 455 m is distinctive, not only because of its low temperature (7.3°C) and salinity (33.8), but also because of its high dissolved oxygen concentration (253 µM) which exceeds even the oxygen concentration in the overlying surface waters. Similar oxygen-rich intrusions have been observed in this region (27.5°N, 145°E) and identified as subsurface mesoscale features forming the North Pacific Central Mode Water (CMW; Oka and Suga, 2005; Oka et al., 2007, 2011). Typically, CMW forms along the subtropical-subarctic frontal zone, eastward along the MWR (Oka et al., 2009). However, the observed CMW-eddy at station 1 was unique with respect to the usual properties of CMW: not only was it oxygen-rich (253 µM), but it was found south of the subtropical front. Because of the similarities in properties between the subsurface CMW eddy described in Oka et al. (2009) and the intrusion observed at station 1 at 455 m, these two features likely result from the same physical mechanism of mesoscale eddy subduction. The second low temperature-low salinity intrusion at 647 m at station 1 (26.9 σ_θ) is interwoven with the lower portion of the Kuroshio Current (527 m; 26.6 σ_θ). In contrast to the oxygen-rich water (253 µM) found at 455 m, the dissolved oxygen concentration at 647 m is lower (107 µM). Despite some differences in temperature and salinity, the potential density at

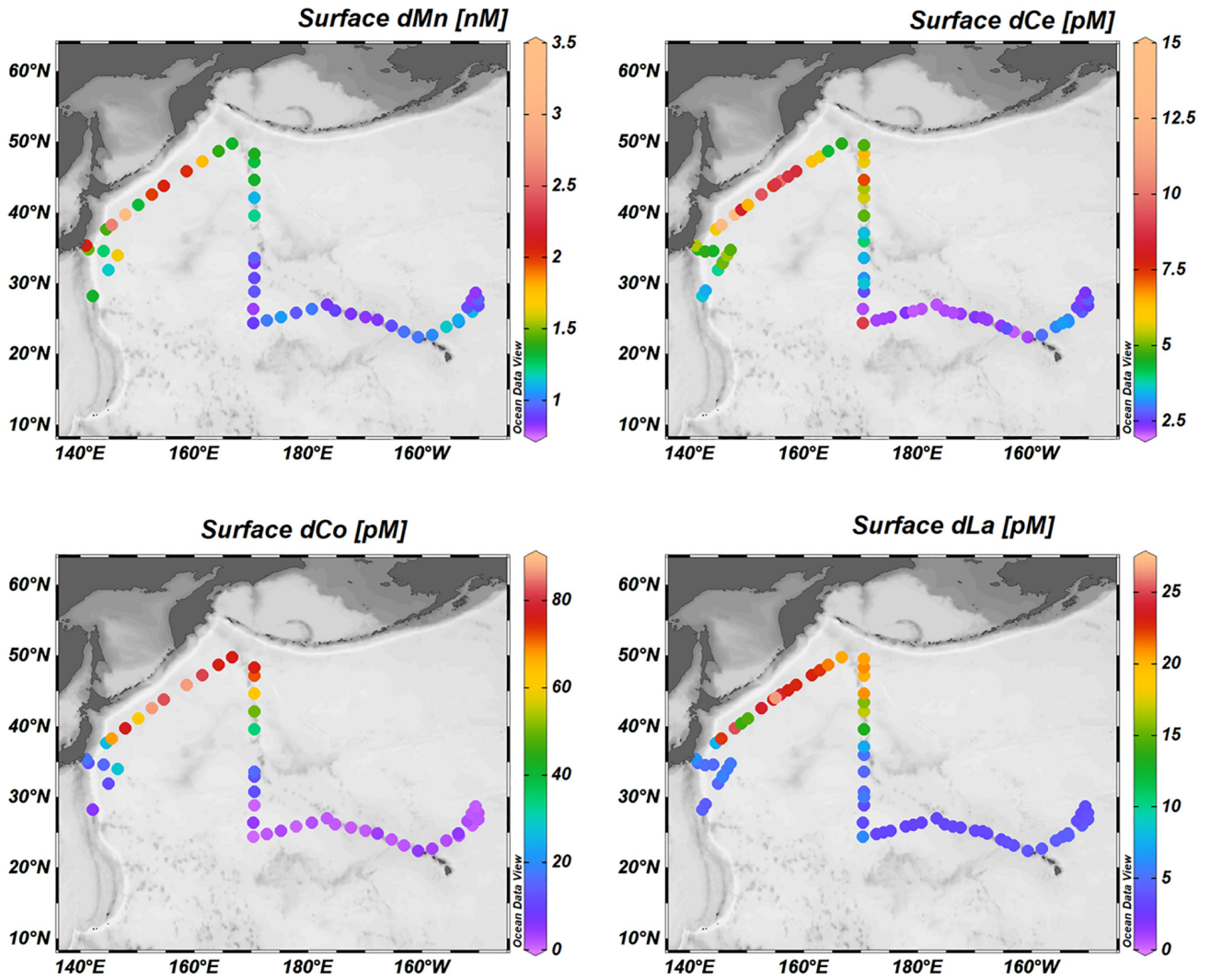

FIGURE 4 | Surface distributions of dissolved trace elements: surface distributions of dissolved Mn, Ce, Co, and La.

647 m (26.9 σ_θ) is similar to that of intermediate waters from the Sea of Okhotsk: the Dense Shelf Water (DSW: ~26.8–27.0 σ_θ) and Okhotsk Sea Intermediate Water (OSIW: ~26.8–27.2 σ_θ) (Andreev and Kusakabe, 2001; Shcherbina et al., 2004). Waters from the Sea of Okhotsk enter the North Pacific at depth through the Kuril-Kamchatka Margin, mix with waters from the WSG and are carried south within the Oyashio Current. Intermediate waters from the Sea of Okhotsk compose ~25% of the Oyashio Current at potential densities of 26.6–27.0 σ_θ (Yasuda et al., 2002), which is within the potential density range of the intrusion at 647 m at station 1.

The dissolved oxygen concentration at 647 m at station 1 likely reflects the mixing of the oxygen-rich intermediate waters from the Sea of Okhotsk (DSW and OSIW) with the oxygen-poor waters of the WSG near station 2 (**Figure 1**). The lower Oyashio Current is comprised of ~25% water from the Sea of Okhotsk and ~75% water from the WSG (Yasuda et al., 2002). If these two waters mix at the proportions suggested by Yasuda et al. (2002), and using the DSW dissolved oxygen concentration of 290–340 μM (Andreev and Kusakabe, 2001) and the oxygen concentrations at the outflow of the Sea of Okhotsk (30–60 μM; station 2), then the predicted oxygen concentrations at 647 m at station 1 would be 95–130 μM. The measured dissolved oxygen concentration of 107 μM at 647 m at station 1 is within this range, and supports a mix of source waters from both the Sea of Okhotsk and the WSG. The vertical profiles of dissolved Mn and Co concentrations at station 1 (**Figure 6**) were clearly impacted by the low temperature-low salinity intrusions at 455 and 647 m. The shallower intrusion at 455 m contains 2.9 nM dMn and 109 pM dCo, while the deeper intrusion at 647 m contains 6.3 nM dMn and 392 pM dCo. Above, below, and between these intrusions were dMn concentrations of 0.65–1.9 nM and dCo at 9.6–87.4 pM, well below the trace metal-enriched waters of the intrusions.

The dREEs concentrations were also high in the shallower intrusion at 455 m and produce a local maximum, with a

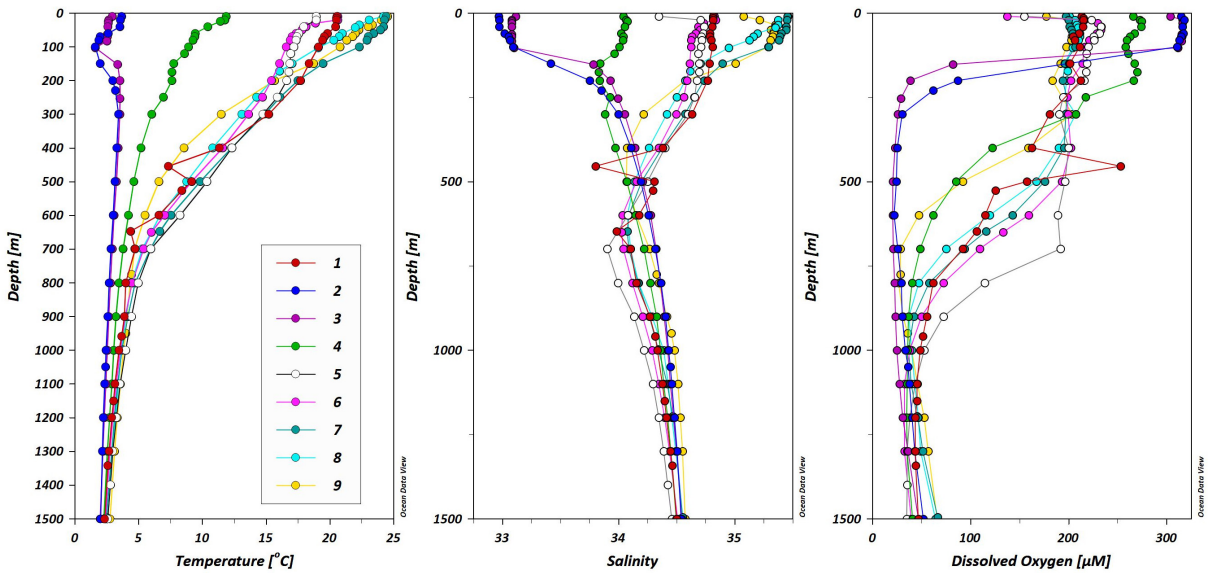

FIGURE 5 | Vertical distributions of physical and chemical properties in the North Pacific Ocean: Vertical distributions of physical and chemical properties in the North Pacific Ocean. Station colors match those in the map (**Figure 1**).

dLa concentration of 23.7 pM, dCe of 102 pM, and dPr of 4.0 pM (**Supplementary Table 2**). Above the 455 m intrusion, the Kuroshio Current waters have lower concentrations of dLa, dCe, and dPr, below the shallow intrusion, the dREEs steadily increase in concentration with depth, but no second maximum at 647 m is observed for any of the light REEs.

The vertical distributions of particulate Mn, Co, and Ce concentrations were also affected by the intrusions at 455 and 647 m (**Figure 7**). Particulate Mn and Ce were highest at 455 m (0.97 nM and 3.1 pM, respectively), while the pCo maximum extended across the entire 455–647 m range (3.1–4.6 pM). Smaller maxima were also observed at 40 m for pCo (2.5 pM) and pCe (0.9 pM).

Kuroshio Extension/Mixed Water Region: Stations 4 (39.3°N, 170.5°E), 5 (33.5°N, 170.5°E), and 6 (30.5°N, 170.5°E)

Stations 4–6 transect the east-west flow of the Kuroshio Extension (**Figure 1**), and the hydrographic features at these stations are a mix of the two contrasting gyres that form the MWR. The upper waters of station 4 (0–200 m) have temperature and salinity values that fall between the subarctic and subtropical gyres (**Figure 5**). Station 4 is midway across the MWR, possessing two small salinity minima at 150 and 300 m. Below these minima (200–1400 m) the temperature and salinity values are similar to those of the WSG stations 2 and 3 in the same depth range. The temperature and salinity at stations 5 and 6 in the upper 400 m are almost identical in structure to station 1 (depths 0–400 m), but also show a broad salinity minimum (300–1400 m) centered at ∼600 m. This salinity-minimum feature spreads across much of the North Pacific Ocean (26.3–26.8 σ_θ; **Figure 8**) and is known as the North Pacific Intermediate Water (NPIW), which forms along the western region of the MWR as a combination of waters from the Sea of Okhotsk, the base of the winter mixed layer in the WSG, and the Kuroshio Current (Qiu, 1995; Talley et al., 1995; You, 2003b, 2005).

The dissolved oxygen concentrations at stations 4, 5, and 6 reflected the incomplete mixing of subarctic and subtropical waters. Stations 4 and 5 had similar high oxygen intrusions like the low temperature/low salinity intrusion at station 1 at 455 m (**Figure 5**), consistent with the continued transport and subduction of WSG waters along the MWR and ongoing formation of the NPIW within the STG. The various intrusions possessed similar physical and chemical properties but were observed at different depths at each station due to the degree of subduction by less-dense Kuroshio waters from the south. Station 4 was located at the northern edge of the MWR, where it was less likely to be influenced by the lower-density Kuroshio waters (from the south) than stations 1 and 5: thus, the CMW was less subducted at station 4 and resided nearer the surface than at the other two stations.

Across the MWR stations, dMn concentrations were highest (1.2–1.6 nM) in the upper 175–250 m (**Figure 6**). A subsurface dMn maximum (1.4 nM) at station 5 at 300 m (25.7 σ_θ) is coincident with the local dissolved oxygen minimum, but not observed at stations 4 and 6. Dissolved Ce concentrations are lowest at 500–650 m at all stations (2.5 pM at station 4, 1.7–1.8 pM at stations 5 and 6), and highest in the upper 300 m (5.0 pM at station 4, 3.0–3.6 pM at stations 5 and 6) but increase with depth (3.4–4.0 pM at 1500 m, stations 4–6). Unlike dMn and dCe distributions, dCo concentrations were lowest at the surface (16–42 pM) and reached mid-depth maxima of 47–55 pM at 300–900 m at stations 4–6. Similar to the dMn at station 5, dCo also showed a shallower maximum at 300 m of

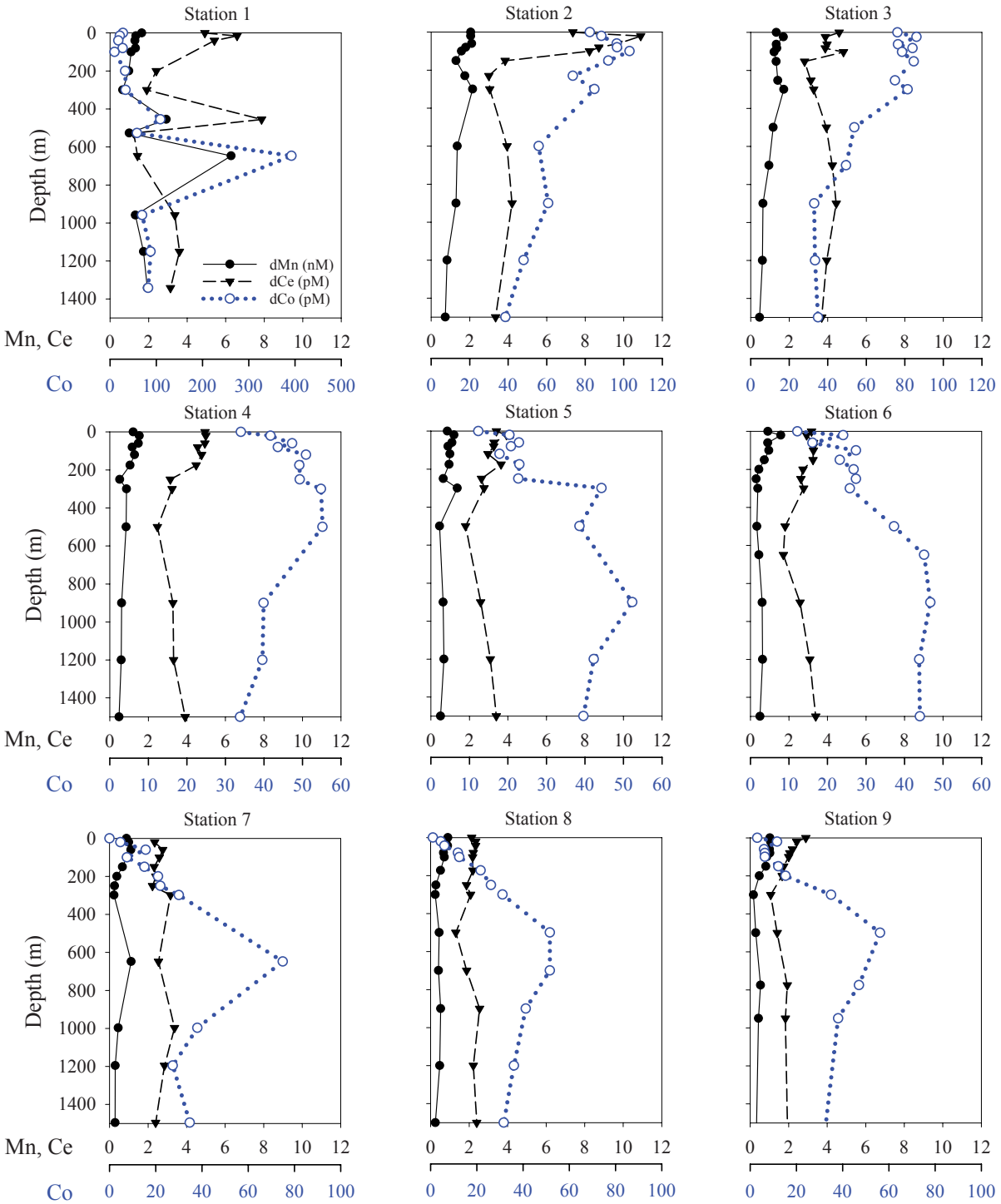

FIGURE 6 | Vertical properties of dissolved trace elements: Vertical profiles of dissolved Mn (nM), Co (pM), and Ce (pM). Note that Co concentration (in blue) scales change depending on the ranges encountered at each station.

44 pM, coincident with the local dissolved oxygen minimum at this station.

Dissolved REE concentrations increased almost linearly with depth at stations 4–6, with upper ocean concentrations decreasing southward across the MWR (**Supplementary Table 2** and **Figure 5**). Concentrations were highest in the upper 500 m at station 4 (dLa = 12.9–20.4 pM, dPr = 2.2–3.0 pM) but decreased

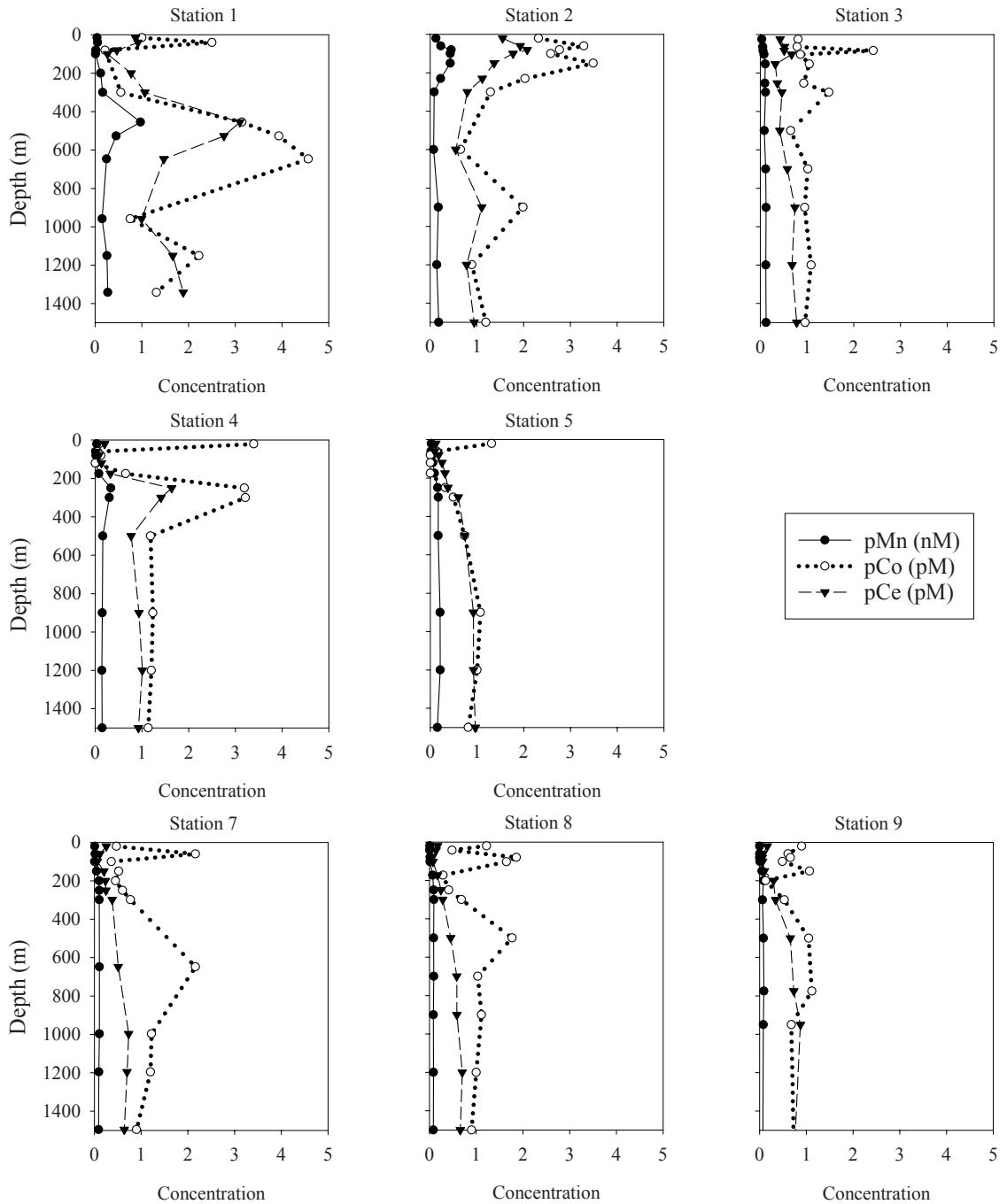

FIGURE 7 | Vertical properties of particulate trace elements: Vertical profiles of particulate Mn (nM), Co (pM), and Ce (pM).

at stations 5 and 6 (dLa = 4.6–11.6 pM, dPr = 0.1–1.8 pM). Below 500 m, dREE concentrations remained relatively constant at all stations (dLa = 30–40 pM, dPr = 3–5 pM).

The vertical distributions of particulate TEs at station 4 were characterized by subsurface maxima at 250–300 m of Mn (0.3 nM), Co (3.2 pM), and Ce (1.6 pM), similar to the dMn and dCo maxima at this same station and depth (**Figure 7**). In contrast, particulate concentrations at station 5 showed a slight surface enrichment for pCo (1.3 pM) but not for pMn or pCe and vertical distributions that slightly increased from low surface concentrations with depth. The particulate concentrations at intermediate depths (500–1500 m) were similar at stations 4 and 5 (pMn = 0.1–0.2 nM, pCo = 0.8–1.2 pM, and pCe = 0.8–1.0 pM). Note that particulate concentrations for station 6 are not

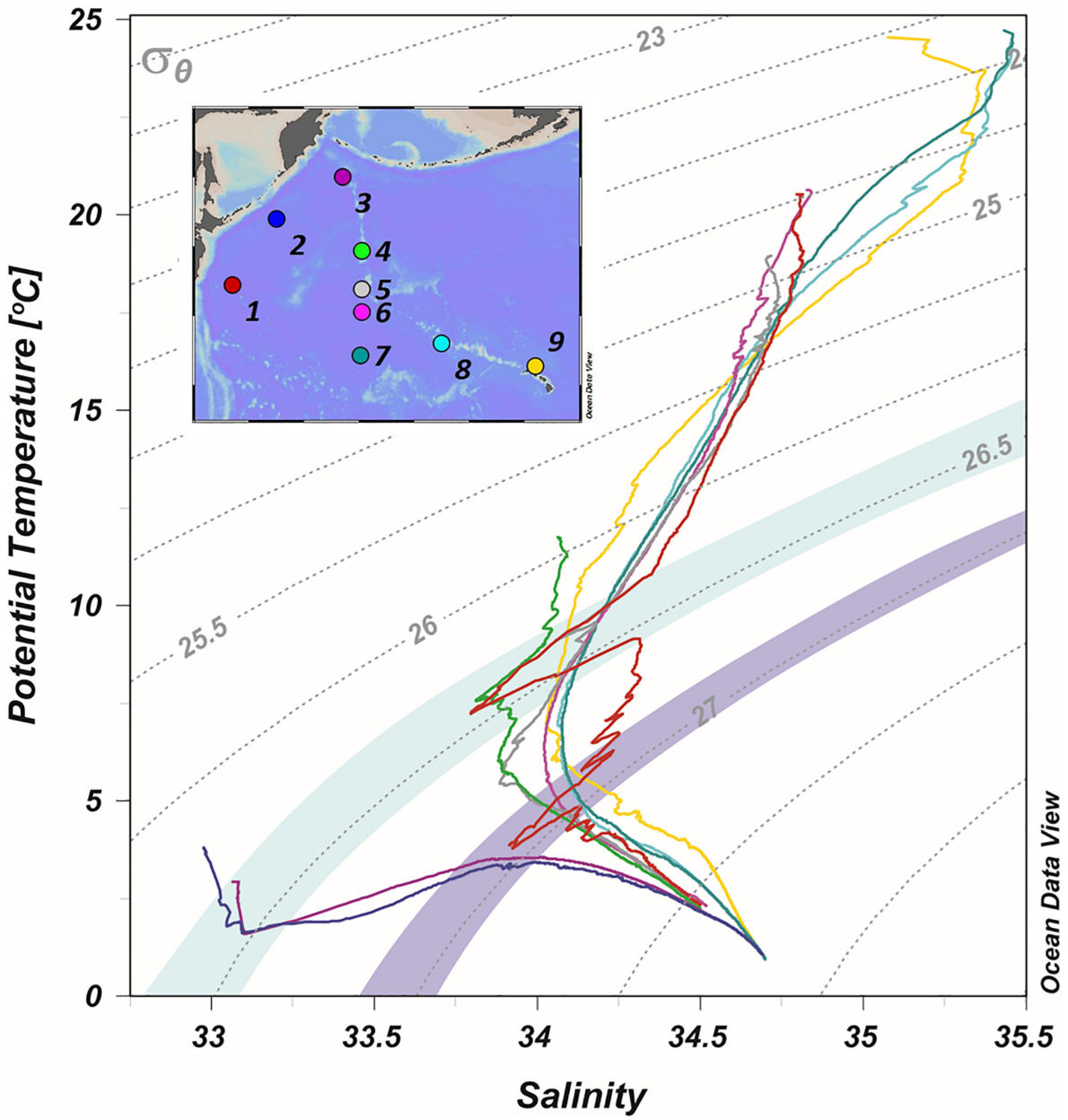

FIGURE 8 | Temperature-salinity profiles for all stations, shown with isopycnal layers (dashed lines). Shaded areas show density ranges for the upper (green, 26.3–26.6 σ_θ) and lower (purple, 26.9–27.1 σ_θ) low temperature-low salinity intrusions.

reported, as these samples were used initially during method optimization trials.

Subtropical Gyre: Stations 7 (24.25°N, 170.3°E), 8 (26°N, 175°W), and 9 (ALOHA; 22.5°N, 158°W)

High temperatures (24–27°C), high salinities (35–35.5), and low densities (23.5–24 σ_θ) characterize the surface waters of the STG. While the WSG is an upwelling region that can supply trace metal-enriched mid-depth waters to the surface, the STG is a downwelling region that depresses the subsurface waters. In the central STG, the most notable water mass is the NPIW, identifiable by a salinity minimum that lies at depths of 400–800 m at potential density surfaces of 26.5–27.5 σ_θ (**Figure 8**).

Dissolved trace element concentrations are influenced by these physical features. Concentrations of dMn were highest (0.7–1.1 nM) in the upper 100 m and decrease to a minimum (∼0.2 nM) at 250 m (**Figure 6**). In general, there was a slight increase in dMn concentrations (0.3–0.5 nM) down to 1500 m, except for a subsurface maximum of 1.1 nM at 648 m at station 7, which was coincident with the salinity minimum at this station. No such feature existed for dMn at stations

8 and 9, but dCo concentrations reached a maximum (52–75 pM) within the salinity minimum at all STG stations. Concentrations of dCo decreased above these maxima to 4–16 pM at the surface and below to 32–35 pM at 1500 m. Dissolved Ce concentrations ranged 1.1–3.4 pM, similar to the concentrations found at depths below 200 m at stations 3–6 (**Figure 6**). However, the vertical profiles lacked any distinguishing features at stations 7 and 8 beyond slightly higher concentrations in the upper 200 m (1.6–2.4 pM) and minimum concentrations (1.1–1.3 pM) at 300–500 m. The vertical profiles of dLa and dPr at all three STG stations were nearly identical: upper ocean (0–300 m) concentrations of dLa were 3.4–7.8 pM which gradually increased to 36–37 pM at 1500 m, and dPr concentrations at 0–300 m were 0.7–1.1 pM increasing to 4.3–4.4 pM at 1500 m (**Supplementary Table 2**).

The STG samples contained some of the lowest particulate concentrations observed in this study (**Figure 7**). Particulate Mn concentrations were less than 0.01 nM in the upper 100 m, increasing to 0.09–0.10 nM at 1500 m. Particulate Ce concentrations were also lowest in the upper 150 m (0.1–0.2 pM) and gradually increase with depth to 0.6–0.9 pM at 1000–1500 m. In contrast to pMn and pCe, vertical distributions of pCo showed some variability throughout the water column, including subsurface maxima (1.1–2.2 pM) at 60–150 m and deeper maxima of 1.1–2.2 pM at all three stations at 500–775 m.

DISCUSSION

Our results are reasonably explained by the release of redox-mobilized dissolved Mn, which is converted *in situ* to particulate Mn. Our discussion is framed by considering the relative importance of each input, removal, and internal transformation term, even though the individual terms cannot be adequately quantified with our data set. The equation summarizing the rate of change in dissolved or particulate trace elements is given in Equation 2,

$$\frac{dC}{dt} = \nabla C + \nabla^2 C + J \quad (2)$$

where dC/dt is the net flux of material (e.g., as nmol m^{-3} d^{-1}), ∇C is the advective flux in three dimensions, $\nabla^2 C$ is the turbulent mixing flux in three dimensions, and J is the change in concentration from internal processes. The J term includes scavenging, settling particles, biological uptake, regeneration, and reduction-oxidation processes. The following sections introduce the different processes involved in the shelf inputs and lateral transport, the evidence for biological Mn-oxide production, the effects of Mn-oxides on Ce and Co cycling, and ultimately their lateral transport across the North Pacific Ocean.

Inputs of Shelf-Derived Redox Active Elements in the WSG

The upper ocean maxima in dissolved and particulate Mn, Co, and Ce in the WSG (station 2, **Figures 6**, **7**) suggest a fluvial, atmospheric, and/or shelf input of material. During the IOC-2002 expedition, the strongest evidence of fluvial material to the North Pacific along our transect was near the Hawaiian islands, where high concentrations of dissolved Fe and Al were concurrent with lower salinity (Brown et al., 2005; Measures et al., 2005), far from the Kuril-Kamchatka margin where the upper ocean plume of Mn, Co, and Ce were observed. Aerosol and surface ocean samples were also examined for evidence of atmospheric deposition of trace metals. Aerosol concentrations of Se and Ag (Ranville et al., 2010), Sb (Cutter and Cutter, 2006), and Pb (Gallon et al., 2011; Zurbrick et al., 2017) indicate that coal combustion from Asia produces aerosols enriched in anthropogenic-derived material. After deposition of these aerosols to the surface ocean, nearshore waters enriched in anthropogenic material can be subducted and advected laterally to produce high dissolved concentrations at intermediate depths, as in the case of Ag (Ranville and Flegal, 2005) and Pb (Zurbrick et al., 2017). While anthropogenic aerosols have been shown to be a source for some metals to the western North Pacific in other studies as well (e.g., Lin et al., 2007; Hsu et al., 2010; Kim et al., 2012), the concentrations of lithogenic tracers like Al (Measures et al., 2005; Buck et al., 2006) and Ga (Shiller and Bairamadgi, 2006) in aerosol and surface ocean samples collected during the IOC-2002 expedition fell below model predictions (Measures et al., 2005; Buck et al., 2006), despite the expedition occupying the western North Pacific during the season of maximum Asian dust inputs. During four dust events encountered during this cruise, concentrations of Fe in aerosols were shown to be highest in the western North Pacific and similar in composition to crustal material, but the aerosol Fe concentrations rapidly diminished with distance from the coast (Buck et al., 2006). Overall, dissolved Fe concentrations in surface waters in the western North Pacific were low (0.1–0.3 nM; Brown et al., 2005), consistent with low atmospheric input and rapid biological uptake in an HNLC region. Therefore, while aerosol inputs are important for some elements in the western North Pacific Ocean, especially those elements enriched in anthropogenic sources, relevant research in this region (even during this same expedition) showed that atmospheric deposition is not as likely to be the primary source of redox-active lithogenic elements in a subsurface plume as a shelf source.

When considering the origin of the subsurface Mn, Co, and Ce plume within the western subarctic gyre (Stations 2 and 3), the supply of trace metals like Fe and Mn from the nearby continental margin has been well documented (Nishioka et al., 2007; Lam and Bishop, 2008; Lamborg et al., 2008; Tanaka et al., 2012; Nishioka and Obata, 2017; Zheng et al., 2019). Our own data support that the shelves are an important source of dMn to the WSG, based on the dissolved and particulate Mn distributions at stations 1–3. At station 2, the upper 600-m can be divided

into three layers: a layer of high dMn in the oxygen-rich surface waters (0–80 m), a pMn plume at 80–150 m that coincides with a sharp oxycline and a localized dMn minimum, and a subsurface dMn maximum that decreases with depth, concurrent with low dissolved oxygen concentrations and the disappearance of the pMn plume (below 150 m). High dMn concentrations extend below the immediate surface waters to 300 m and show a double maximum (**Figure 9**), near the surface (0–60 m) and below the oxycline (200–300 m). As dMn is released from the sediments of the Kuril-Kamchatka margin (Lam and Bishop, 2008), it can undergo redox transformations at the sediment-water interface and/or during transport to the WSG. Centered between the two dMn maxima is a maximum in pMn (80–150 m, 0.44 ± 0.01 nM) that overlaps the oxycline (100–230 m) and could result from resuspension of shelf-derived material, scavenging, or biological uptake or oxidation of dMn. Above the pMn maximum, dMn is likely sustained in the surface (0–80 m) by photochemical reactions with dissolved organic carbon that either inhibit the formation of pMn or transform pMn to dMn through reductive photochemical dissolution (Sunda, 2012; Hansel, 2017). Below the pMn maximum (150–300 m), low oxygen concentrations prevent Mn oxidation, and so the dMn plume originating from the margin persists. Furthermore, the pMn plume at 80–150 m is 20–25% of the total Mn (dMn + pMn), and the depth-integrated concentration of pMn over the upper 300 m is 82.9 μmol m^{-2}, which closely matches the "missing" depth-integrated (80–150 m) dMn concentration of 104.7 μmol m^{-2}. Noticeably absent from the upper 600-m is any indication of a concurrent pTi plume (**Supplementary Table 2**), which would indicate offshore transport of atmospheric or marine resuspended lithogenic (i.e., non-redox mobilized) material.

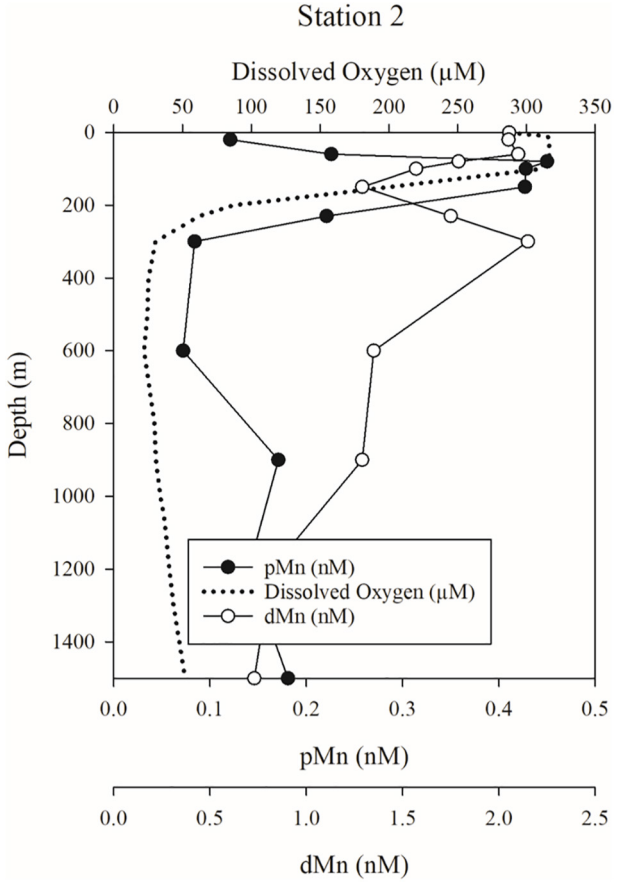

FIGURE 9 | Dissolved (dMn) and particulate Mn (pMn) profiles with dissolved oxygen concentrations at station 2.

Enrichments of Mn, Co, and Ce and the Composition of the pMn Plume

The composition of the pMn plume can be better identified by comparing against a crustal tracer like pTi. In the pMn plume at 80–150 m station 2 (**Figure 10**), the pMn/Ti ratio is roughly tenfold higher than crustal abundance (1.7–2.5 mol Mn/mol Ti at 80–150 m, vs. an average crustal abundance value of 0.18 mol Mn/mol Ti, Rudnick and Gao, 2003). This enrichment suggests that the pMn is not simply a result of the resuspension of sedimentary material or atmospheric deposition of crustal material, but more likely is produced during lateral transport of dMn released from the shelf. Microbial processes capable of oxidizing dMn are well-documented (Moffett and Ho, 1996; Bargar et al., 2000; Tebo et al., 2004; Dick et al., 2008; Spiro et al., 2010; Toyoda and Tebo, 2016), and these same microbes or the Mn-oxides they produce can also scavenge and/or oxidize dCo and dCe (Tebo et al., 1984, 2004; Moffett, 1990, 1997; Moffett and Ho, 1996; Learman et al., 2011; Schijf et al., 2015; Hansel, 2017). At station 2, the maxima of particles enriched in Co and Ce (based on the vertical profiles of pCo/Ti and the pCe anomaly) coincide with the pMn/Ti maximum within the oxycline. When all the facts are considered in concert – the concurrence of the localized dMn minimum with the pMn maximum at station 2; the lack of evidence of a plume of resuspended lithogenic particles; the coincidence of the pMn, pCo, and pCe enrichments; and the extensive documentation of biological Mn oxidation and its influence over other trace element cycles – the natural conclusion is that the pMn plume is composed of Mn-oxides, biologically produced from dMn originating from the nearby shelf.

Particulate Mn Removal via Settling Particles

The pMn plume could be lost from the upper ocean as settling particles, as was observed by Lamborg et al. (2008). Concentrations of trace elements like Mn and Al were determined in settling material collected in sediment traps at station K2 (47°N 160°E; Lamborg et al., 2008) which is near our station 2 (44°N 155°E). While the analytical and natural variability prevent a more precise estimate of the sediment trap particle composition, the estimated Mn/Al ratios in the sediment traps at K2 suggest that the settling particles are approximately three times enriched over crustal abundance, and our own suspended particles at station 2 are enriched tenfold over crustal abundance (relative to Ti). The differences in enrichment could be due to spatial variations, temporal variations (K2: June-July 2004; station 2: April 2002), filter pore size (K2: 1.0 μm; station

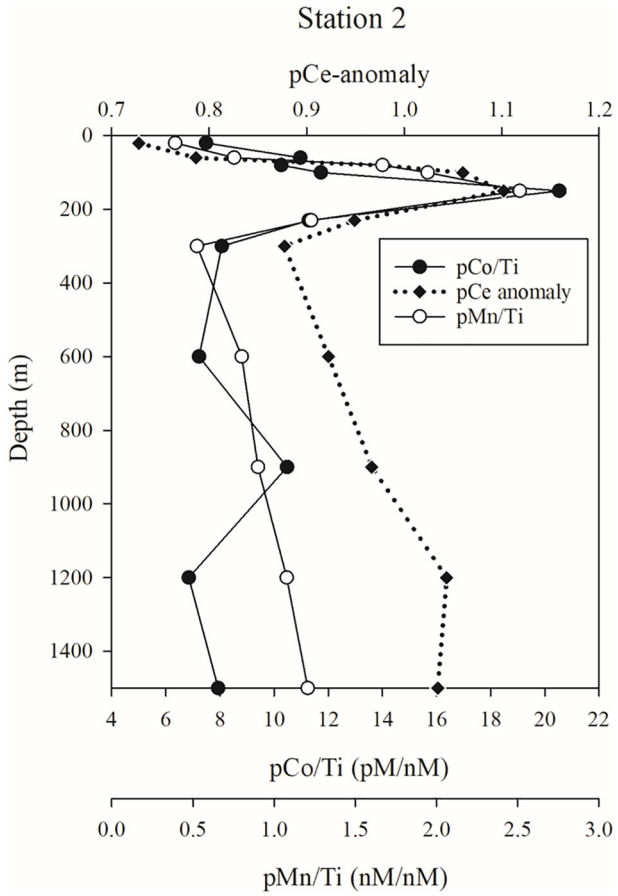

FIGURE 10 | Enrichments of particulate Mn (pMn/Ti), Co (pCo/Ti), and Ce (pCe anomaly) over crustal abundances.

2: 0.4 μm), or even reductive dissolution or desorption of settling particles as they pass through the low oxygen waters below 300 m (**Figure 9**). Regardless of the differences, both the suspended particles at station 2 and the settling particles from K2 are enriched in Mn and suggest that some fraction of the pMn-oxides are indeed lost by settling.

Therefore, the extent of lateral transport of the Mn plume depends on the contrast between the settling rate of pMn and current velocity that can advect the shelf-derived material offshore. The residence time of the pMn plume can be estimated using the depth-integrated concentration at station 2 and the sediment trap settling fluxes at K2 (Lamborg et al., 2008). The depth-integrated pMn concentration in the upper 150 m at station 2 is 46 μmol m^{-2}, and the range of settling fluxes at nearby station K2 is 111 ± 67 nmol m^{-2} day^{-1} from neutrally buoyant sediment traps (NBST) and 175 ± 117 nmol m^{-2} day^{-1} from surface tethered "CLAP" traps (Lamborg et al., 2008). The resulting residence time of pMn at station 2 is 415 ± 251 days (NBST) or 265 ± 177 days (CLAP). This pMn residence time exceeds the 54–108 days required for the Oyashio Current to travel from station 3 to station 1 (1860 km), assuming a velocity of 0.2–0.4 m/s (Ohshima et al., 2005), allowing the concentrations of pMn (and other elements associated with the Mn particles) to accumulate within the Oyashio waters and be transported offshore.

Dissolved and Particulate Ce-Anomalies

The influence of Mn-oxides over dissolved and particulate REE distributions can be explored by considering both the dissolved and particulate Ce anomalies at station 2. The dCe (**Figure 6**) and pCe concentrations (**Figure 7**) are highest in the upper 300 m at station 2, while dissolved concentrations of La and Pr are lowest at the surface and steadily increase with depth (**Supplementary Table 2**). While an atmospheric source of this surface maximum of Ce (and other REEs) might be plausible, the dissolved and particulate Ce anomalies argue against an atmospheric source of lithogenic material. The dCe anomaly (normalized to PAAS) is overall depleted (0.05–0.25) throughout the upper 500 m (**Figure 11**). Our dCe anomalies compare favorably with those from VERTEX IV (28°N, 155°W; de Baar et al., 2018): the upper waters are similarly depleted, with the highest dCe anomaly of 0.22–0.35 in the upper 150 m, declining quickly to a dCe anomaly of 0.05 by 500 m. This overall depletion indicates that dCe is being preferentially removed relative to dLa and dPr. A likely mechanism for this removal is via oxidation by pMn-oxides or Mn-oxidizing microbes, as evidenced by the pCe anomaly which coincides with the pMn/Ti maximum (**Figure 10**), which could oxidize dCe to particles that are removed by settling. Furthermore, the dCe anomaly is highest near the surface, coincident with the surface maximum in dMn, but in contrast no such dCe anomaly is observed with the deeper dMn maximum (150–300 m). The contrast between dCe and dMn is consistent with a supply of dMn that is oxidized to pMn during offshore transport. Particulate Mn-oxides are prohibited from forming or are photochemically dissolved near the surface (Sunda et al., 1983; Sunda and Huntsman, 1988, 1994), which in turn would prevent the subsequent oxidation of dCe to pCe oxides in the upper 80 m at station 2. Within the pMn plume (80–150 m), the dCe is oxidized and forms particles enriched in Ce relative to La and Pr, thus producing the pCe anomaly maximum. Below the pMn plume, pMn oxides are transformed to dMn through reductive dissolution in the low oxygen conditions, but pCe appears to be unable to dissolve as quickly as pMn oxides and is therefore likely lost as settling particles from the upper ocean. The production and removal of Ce-enriched particles steadily depletes the dCe relative to the other dREEs. Therefore, the upper 300 m waters are also depleted in pCe (which are produced in dCe-depleted source water) except at the pMn maximum, due to preferential oxidation and scavenging of redox-mobilized dCe from the shelf and exacerbated by low inputs of lithogenic material from atmospheric or resuspended shelf sources.

Biological Controls Over Particulate Co

Biological demand also influences the distributions of trace metals like Co in the WSG. While Mn is a bioactive trace metal, its concentrations are usually found in excess of biological demand and therefore are not considered limiting (Sunda and Huntsman, 1996, 2000; Morel et al., 2003). Cobalt also plays a critical biological role in marine microbes, as an essential trace

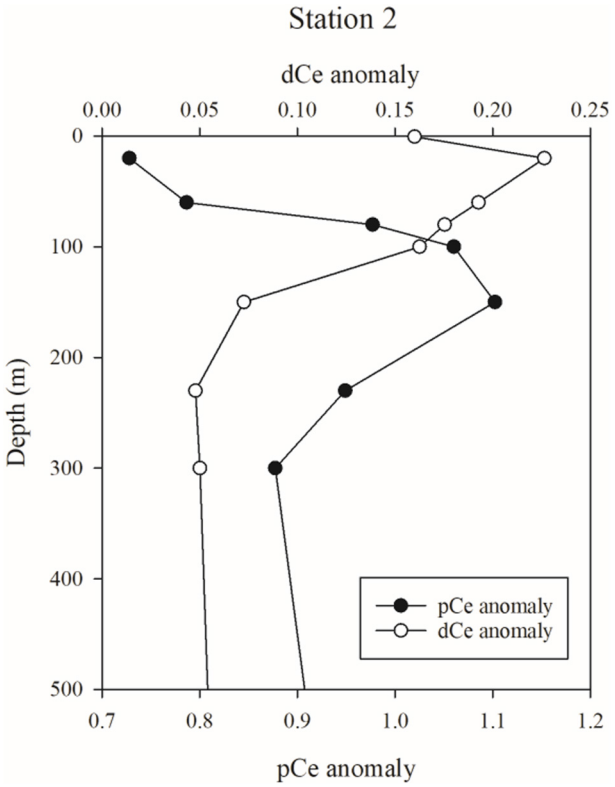

FIGURE 11 | Dissolved (dCe) and particulate Ce (pCe) anomalies at station 2, showing the vertical offsets and differing scales between the two phases.

nutrient for carbonic anhydrase and cobalamins, for example (Morel et al., 2003; Saito et al., 2005), but its concentrations are much lower than those of dMn. As such, dCo is often observed to be complexed with strong organic ligands in the open ocean, thus preserving its solubility and potential bioavailability (Ellwood and van den Berg, 2001; Saito and Moffett, 2001; Noble et al., 2017; Tagliabue et al., 2018). The dissolved-particulate partitioning of Mn and Co at station 2 is evidence of these differences, where pMn constitutes up to 25% of the total Mn, while the pCo is only a small fraction of the total Co (2–6%), likely due to an oxidized form [i.e., Co(III)] that is soluble (Moffett and Ho, 1996) and complexed by organic ligands (Noble et al., 2012). The vertical profile of pCo concentrations features two maxima in the upper 300 m (**Figure 7**): the shallower maximum at 60 m coincides with the chlorophyll *a* maximum in the upper 50 m (Measures et al., 2006) while the deeper maximum at 150 m coincides with the pMn/Ti maximum, suggesting co-oxidation with Mn oxides like Ce. Below 150 m, the pCo concentrations rapidly decrease across the oxycline, but dCo concentrations are slightly elevated at 300 m, consistent with the desorption and reductive dissolution of dCo from the pMn-oxides through the oxygen minimum zone. In summary, it is likely that the pCo profile reflects influences by active biological uptake by phytoplankton (50–60 m) and scavenging (and possibly oxidation) by pMn-oxides at 80–150 m. However, the majority of the dCo originating from the shelf with dMn and dCe is preserved in the dissolved fraction, probably due to the combined effects of an oxidized form that is soluble and the prevention against particulate scavenging and loss by organic ligands.

Lateral Transport of Shelf Material From the WSG

Material supplied to the WSG from the shelf is transported by ocean currents far beyond the source. The Oyashio Current travels along the Kuril-Kamchatka margin from north to south (station 3 to 2) and then collides with the Kuroshio Current coming up from the south (station 1), gradually mixing eastward along the MWR (transected by stations 4–6) and into the central subtropical gyre (stations 7-9; **Figure 1**). This region between the Oyashio and Kuroshio is known as the MWR for good reason: the confluence of the currents generates numerous surface and subsurface eddies as well as mode and intermediate water masses which can travel throughout the western and central North Pacific Ocean (Talley and Yun, 2001; Mitsudera et al., 2004; You, 2005; Oka et al., 2009; Oka and Qiu, 2012). Depending on the relative rate of transport and removal, waters subducted in the WSG will carry with them any dissolved or particulate material introduced prior to their subduction.

Enrichment of Trace Element Concentrations in WSG Currents

The oxygen-rich waters transported out of the WSG are also rich in dissolved and particulate Mn (**Figure 12**). Upon encountering the Kuroshio Current at station 1, the parcel at 26.4 σ_θ is subducted from ∼150 m in the WSG to 455 m at station 1, while the parcel at ∼27 σ_θ is subducted from 300 m in the WSG to 647 m at station 1. The water parcel at 26.4 σ_θ increases in both dMn and pMn concentrations as well as the pMn/Ti enrichment from north to south (from station 3 to 2 to 1), consistent with ongoing inputs of redox-mobilized shelf material and *in situ* microbial oxidation. The lower parcel at ∼27 σ_θ is enriched in dMn but not pMn, as these waters originated below the oxycline and within the oxygen minimum zone. The lower rate of Mn scavenging in the low oxygen waters may have preserved the shelf inputs of Mn in the dissolved state and also dissolved some portion of the settling pMn-oxides. Concentrations of both dMn and pMn continued to accumulate along the shelf until reaching the maximum observed concentrations at station 1.

Cobalt and Ce were also transported along this same pathway (**Figure 13**). In the 26.4 σ_θ parcel, concentrations of dCo remained almost unchanged, from 103 pM at station 2 to 109 pM at station 1, but dCo concentrations increased greatly in the 27 σ_θ parcel, reaching a concentration of 392 pM at station 1. The lack of a dCo increase between stations 3 and 2 at 27 σ_θ indicates that the source of dCo at these depths is a lateral input located further downstream of station 2, likely generated during the turbulent outflow of intermediate waters from the Sea of Okhotsk (Yasuda et al., 2002; Yasuda, 2004). Similar enrichments of trace metals by this mechanism have been observed for Fe (Nishioka et al., 2007) and possibly even Hg (Laurier et al., 2004). As the 27 σ_θ water mass continues southward beyond the

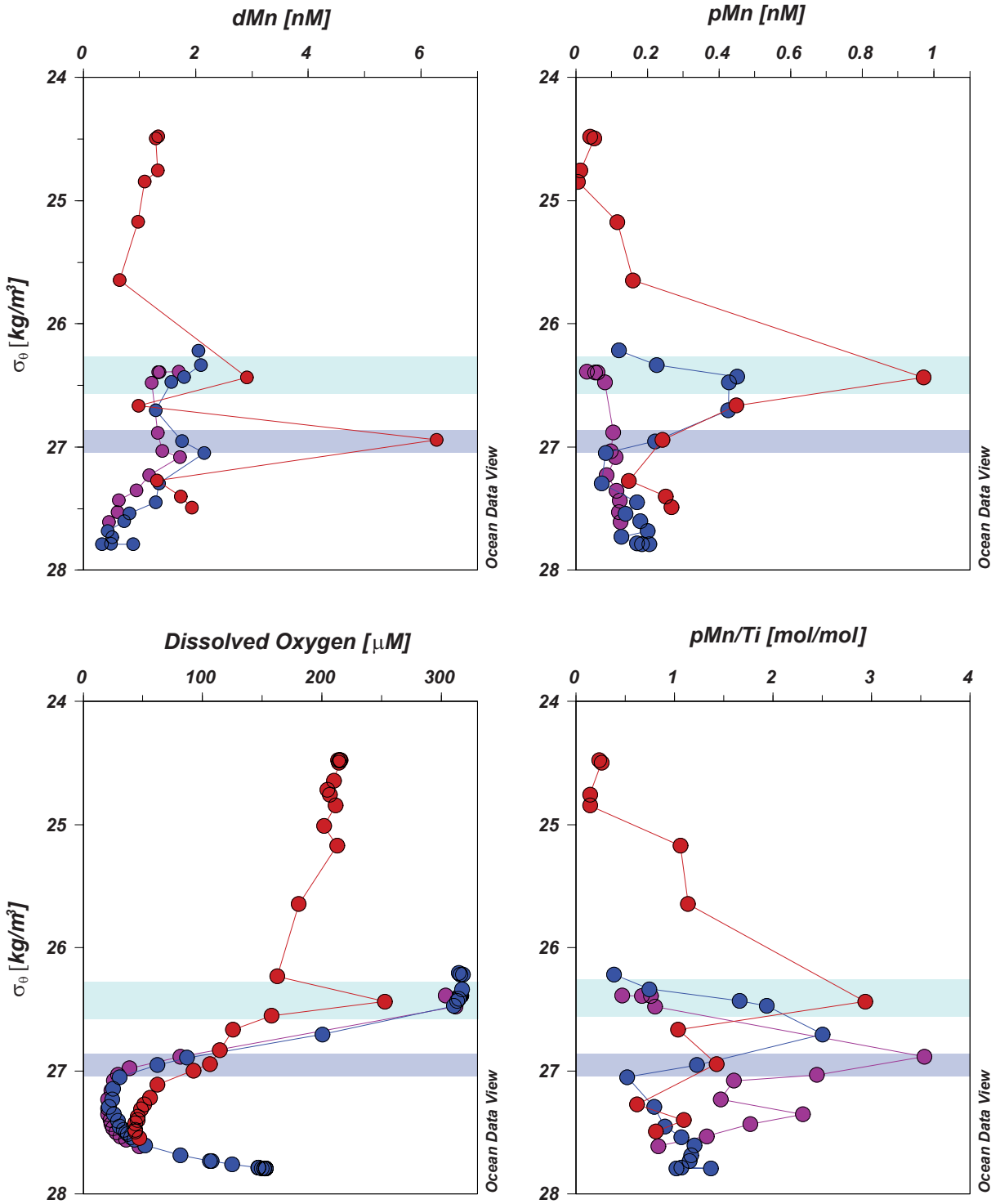

FIGURE 12 | Margin inputs of Mn in the WSG: Transport of Mn from the WSG, with increasing dissolved and particulate concentrations with increased contact time with the Kuril-Kamchatka margin. Note that the greatest increases occur along the 26.4–27.3 σ_θ isopycnal surfaces, consistent with inputs from the Kuril-Kamchatka Margin and intermediate waters from the Sea of Okhotsk. Shaded areas show density ranges for the upper (green, 26.3–26.6 σ_θ) and lower (purple, 26.9–27.1 σ_θ) low temperature-low salinity intrusions.

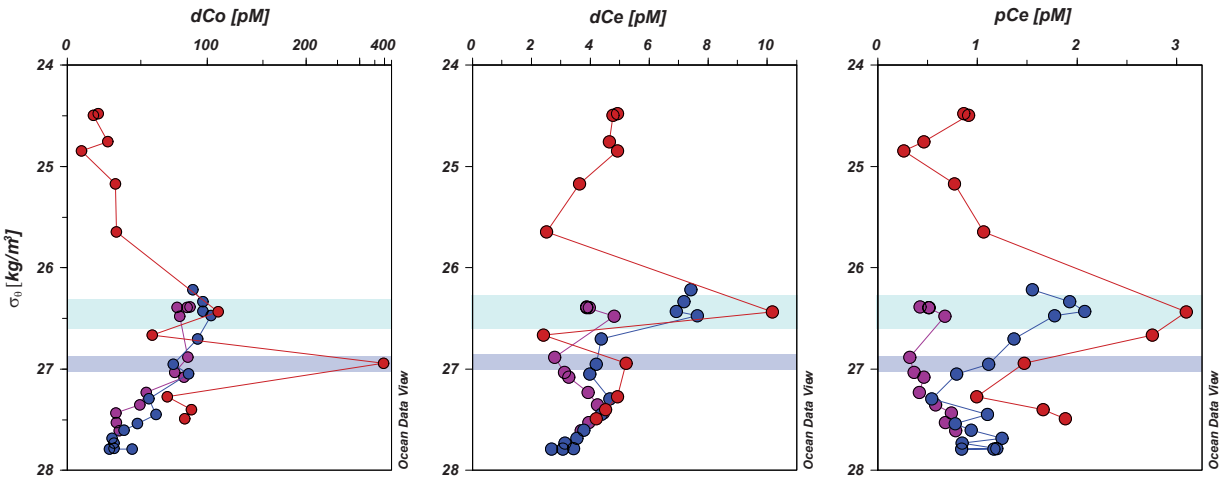

FIGURE 13 | Margin inputs of Co and Ce in the WSG: Elevated concentrations of dissolved and particulate Co and Ce in the 26.4 σ_θ water mass resulting from lateral inputs from the nearby margin. Shaded areas show density ranges for the upper (green, 26.3–26.6 σ_θ) and lower (purple, 26.9–27.1 σ_θ) low temperature-low salinity intrusions.

extent of our sampling locations (You, 2005), the distinctive trace metal properties of this feature have remained largely unexplored except for its influence on the formation of the North Pacific Intermediate Water (NPIW) encountered throughout the central North Pacific Ocean (stations 6–9).

Shelf Fluxes to the WSG

The shelf fluxes of Mn, Co, and Ce to the WSG can be estimated using the increase in concentrations from station 3 to 1 (1860 km), assuming a current velocity of 0.2–0.4 m s^{-1} for the Oyashio Current (Ohshima et al., 2005). Within the 26.4 σ_θ water mass, the dMn concentrations increase from 1.34 nM to 2.91 nM, an increase of 1.57 nM over 54–108 days. The resulting flux of dMn from the shelf along the 26.4 σ_θ isopycnal is 5.3–10.6 nM yr^{-1}. Similarly calculated, the pMn shelf flux is 3.1–6.2 nM yr^{-1}. Fluxes of dissolved and particulate Co are 96.2–192.3 pM yr^{-1} and 7.9–15.8 pM yr^{-1}, respectively, and fluxes of dissolved and particulate Ce are 21.2–42.3 pM yr^{-1} and 8.7–17.4 pM yr^{-1}.

Offshore Transport of Trace Elements

The Oyashio and Kuroshio Currents turn eastward near station 1, away from the supply of trace elements from the shelf. At stations 4 and 5, water masses with low salinities and high dissolved oxygen concentrations are observed within the same isopycnal range as the two intrusions observed at station 1 (**Figures 5**, **8**). While maxima in pMn and pCe are observed at 250–300 m at station 4 (26.6–26.7 σ_θ), no other particulate maxima are observed within these depths and density ranges at the other STG stations. In contrast, pCo maxima are found at stations 4 and 7–9 at intermediate depths (300–800 m).

The dissolved concentrations of Mn also decrease with distance from the shelf, remaining at concentrations near 1 nM (0.8–1.6 nM) in the upper 300 m (**Figures 4**, **6**). The concentrations of dMn in the upper ocean can be resupplied by episodic atmospheric deposition (Buck et al., 2013) and/or the photochemical inhibition of oxide production in the surface waters (Sunda and Huntsman, 1988, 1994; Moffett, 1994b, 1997) which would prevent the loss of Mn by particle scavenging. This lack of Mn oxidation could also suppress the conversion of dCe to pCe-oxides through scavenging and co-precipitation with pMn-oxides. While the cycles of Mn, Co, and Ce might be coupled near the shelf, subtle differences in their biogeochemistry should become more apparent once the water masses containing shelf-derived material move further from the shelf source.

Rate of Particulate Trace Element Loss With Offshore Transport

Moving offshore along the 26.4 σ_θ isopycnal surface from station 1 to stations 4 (300 m) and 5 (500 m), there is no more shelf supply of dissolved trace elements to the water mass. Without the additional supply of dissolved material, the dissolved Mn, Co, and Ce should decrease due to ongoing scavenging and co-oxidation with pMn. The rates of loss of Mn, Co, and Ce can be estimated by assuming that the conversion of dissolved to particulate phases is the rate-limiting step, is first order using Equation 3

$$A_t = A_0 e^{-kt} \quad (3)$$

where A_t is the final concentration at station 4 or 5, A_0 is the original concentration at 455 m at station 1, and t is the travel time from station 1 to stations 4 or 5. While the Kuroshio Current is a fast-moving western boundary current (0.7–1.0 m s^{-1}; Mitsudera et al., 2004), we apply a more modest velocity of 0.2–0.4 m s^{-1} for the offshore extension of the Kuroshio. The dMn decreases from 2.91 nM at station 1 to 0.86 nM and 0.45 nM at stations 4 and 5, respectively, and result in a Mn loss rate of 0.10–0.30% d^{-1}. Similarly, the Ce loss rate is 0.09–0.28% d^{-1}, closely matching that of Mn and supporting their concurrent removal. These rates are lower than the estimated oxidation rates of Mn (2–3% d^{-1}) and Ce

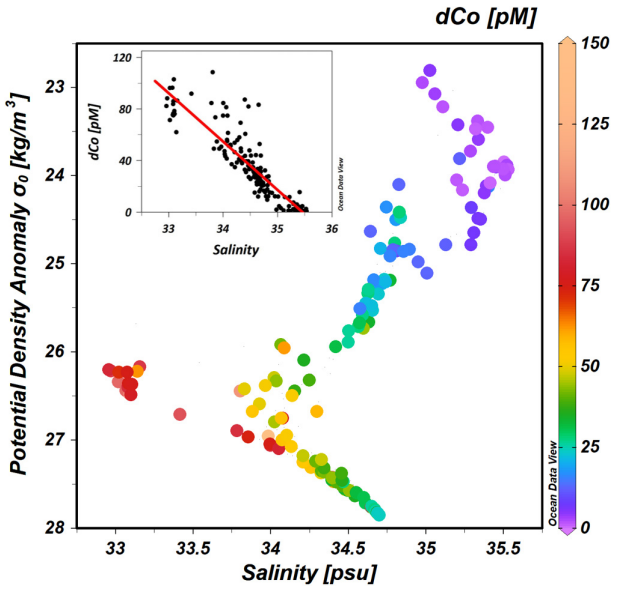

FIGURE 14 | Dissolved Co in the NPIW: The highest concentrations of dCo (pM) are found in the lowest salinity water and in the 26.0–27.3 σ_θ isopycnal range. Linear regression line of dCo and salinity is described by the equation [dCo (pM)] = (–37.8 ± 1.6) × (salinity) + (1325 ± 55); r^2 = 0.789.

(0.3–0.8% d^{-1}) reported by de Baar et al. (1988) and Moffett (1990), respectively. Moffett (1990) also noted that marine Mn oxidation rates were 3–4 times faster than Ce oxidation rates, in contrast to our similar dissolved Mn and Ce loss rates. Therefore, our dissolved trace element loss rates are likely not accurate estimates of oxidation rates, but include other processes such as scavenging and particle settling that were not incorporated in the direct measurements made by Moffett (1990). The loss rate of dCo (0.05–0.17% d^{-1}) is about half of the Mn or Ce loss rate, suggesting that while co-oxidation with Mn-oxides is occurring, other processes such as biological uptake and organic-complexation act to decouple the Co cycle from those of Mn and Ce. In summary, the loss of dMn and dCe are likely to continue through scavenging and microbially mediated oxidation after leaving the shelf. This ongoing conversion of dMn and dCe to settling particles is in contrast to the preservation of Co in the dissolved phase, observable as a subsurface maximum associated with the salinity-minimum core of the NPIW across the North Pacific Ocean (Noble et al., 2008; Zheng et al., 2019).

Trace Elements in the NPIW

The partially mixed waters at station 1 from 455 to 647 m are the precursor of the NPIW, which forms with a core potential density of ~26.8 σ_θ (26.5–27.5 σ_θ) from the Kuroshio Current and waters from the WSG, including contributions from both the Oyashio Current and the Sea of Okhotsk (Talley et al., 1995; Yasuda et al., 2002; You, 2005). The changes in temperature and salinity within this potential density range of 26.5–27.5 σ_θ, from the WSG (stations 2 and 3) across the MWR (stations 1, 4–6) and into the central North Pacific (stations 7–9), show the gradual mixing of multiple water masses to form a single water mass – the NPIW – with a characteristic mid-depth salinity minimum. Evidence of the long-range transport of coastal material, including Fe, Hg, and terrestrial DOC, from the Sea of Okhotsk and the WSG, has been found within the NPIW (Hansell et al., 2002; Hernes and Benner, 2002; Tani et al., 2003; Nakatsuka et al., 2004a,b; Nishioka et al., 2007; Misumi et al., 2011; Hammerschmidt and Bowman, 2012; Tanaka et al., 2012).

The widespread distribution and temporal variability of dissolved trace element distributions in the NPIW can be observed in comparisons with similar studies conducted near our IOC2002 station 9 (ALOHA). Dissolved Mn concentrations at ALOHA and nearby locations in the STG are compared in **Figure 2** and show a variable but persistent surface maximum that overlies a subsurface minimum around 300 m (Martin et al., 1985; Landing and Bruland, 1987; Boyle et al., 2005; Noble et al., 2008; Zheng et al., 2019). Dissolved Ce concentrations are consistently low, ranging from 1 to 5 pM (Fröllje et al., 2016), with a slight surface maximum but no other obvious structure throughout the water column, even at sites further from ALOHA (EUC-Fe station 14 at 0°N, 180°W; Grenier et al., 2013). Unlike dMn and dCe, the concentrations of dCo remain high (maxima near 40–80 pM) in the 300–1000 m range across the MWR and STG (stations 4–9; **Figure 6**). Similar features in dCo have been reported in waters to the southwest of the Hawaiian islands (Noble et al., 2008) with a subsurface maximum observed at depths of 400–600 m (**Figure 2**) and a potential density range of 26.5–27.0 σ_θ. A recent high-resolution section along 160°W further illustrates the extent of this intermediate water dCo maximum, where high dCo concentrations are observed throughout the NPIW at 400–600 m depth, from 25 to 45°N (Figure 3 of Zheng et al., 2019). When comparing the vertical profiles of dCo concentrations from our IOC2002 expedition with the nearby stations from Noble et al. (2008) and Zheng et al. (2019), the subsurface dCo maximum within the NPIW is observed in all profiles shown in **Figure 2** but the magnitude of the maximum itself exhibits some variability. The maximum dCo concentrations observed in the NPIW range from 56.2 pM at station ALOHA (IOC2002 Stn 9) to 84.1 pM at stations to the southwest of the islands (E-Flux III, In 3; Noble et al., 2008). Note that lower dCo concentrations were observed at stations immediately to the north (Zheng ST07) and south (Zheng ST08) of IOC2002 station 9 (ALOHA) by Zheng et al. (2019), due to incomplete Co recoveries resulting from the lack of a UV-oxidation step which liberates organically complexed Co. However, assuming that dCo concentrations without UV-oxidation are ~60% of those obtained with UV-oxidation (as noted in the 2013 SAFe Co report), the concentrations reported by Zheng et al. (2019) at their stations ST07 and ST08 would be ~70 pM and comparable to the concentrations found in the other nearby studies. In addition to variations in the biogeochemical processes along the shelf (sedimentation rates, organic carbon remineralization, etc.) as well as biological uptake and scavenging

rates of dCo offshore, the variations in NPIW dCo concentrations also partially result from annual and seasonal meanders of the Kuroshio Current and Extension and the hydrography of the western subarctic gyre (Bograd et al., 1999; Kinugasa et al., 2005; Oka et al., 2007; e.g., Talley et al., 1995; You, 2003a, 2005; Yasuda, 2004; Qiu and Chen, 2005): each of these circulation patterns directly affect the formation of the NPIW, and subsequently the horizontal distribution of dCo across the central North Pacific Ocean.

The characteristic salinity minimum of the NPIW makes an ideal tracer for testing the hypothesis that dCo is supplied from the margins to the WSG. Other studies have shown strong relationships between dCo and salinity in the northeast Pacific Ocean (Knauer et al., 1982) and the north and south Atlantic Ocean (Saito and Moffett, 2002; Dulaquais et al., 2014). The surface salinities of the WSG are distinctively low (**Figure 3**), and comparing dCo against salinity across the entire study region reveals that dCo concentrations in the western North Pacific are negatively correlated with salinity (**Figure 14**), and the relationship can be described by the linear equation [dCo] = $(-37.8 \pm 1.6) \times$ (salinity) + (1325 ± 55) (R^2 = 0.789; excluding the highest concentration of 392 pM from the 647 m Okhotsk Sea intrusion at station 1). The strength of the relationship between dCo concentrations and salinity supports our conclusion that the Sea of Okhotsk and the WSG are the primary sources of dCo found in the NPIW, transporting dCo at intermediate depths throughout much of the North Pacific Ocean.

CONCLUSION

Evidence for margin inputs of Mn, Co, and Ce to the western North Pacific was found along the Kuril-Kamchatka margin. A comparison of the redox active elements Mn, Co, and Ce with the hydrography of the western North Pacific revealed an extensive transport system capable of advecting margin-derived material along surface and intermediate water masses far beyond the immediate continental shelf. Both redox-mobilized and resuspension processes were identified through particulate elemental ratios, which allowed for better identification of the processes responsible for the trace metal distributions. In summary, physical ocean processes can have a tremendous influence on both the input and transport of trace metals.

The significance of margin inputs goes beyond that of dMn supply to the western North Pacific. The biogeochemistry of other bioactive trace metals can be influenced by the transformation of dMn to pMn, and the transport of both phases when entrained into water masses. While Co and Ce can be microbially oxidized using the same biochemical pathway as that of Mn (Moffett, 1994b; Moffett and Ho, 1996), our results can also be explained by the scavenging and oxidation of Co and Ce by the Mn-oxides themselves (De Carlo et al., 1997; Tebo et al., 2004). Due to the reactivity of the Mn oxide phases, it is possible that the cycling of Mn could affect other trace metals in addition to Co and Ce, through scavenging, oxidation, and/or reductive dissolution.

The physical circulation is also critical to the transport of redox active elements from the shelf to the open ocean. The Sea of Okhotsk is a region of seasonal sea-ice formation and brine rejection, which influence the densities, depths, and intensity of surface and intermediate waters circulating in the WSG. Long-term disruptions of sea ice formation in the Sea of Okhotsk (Paik et al., 2017) will subsequently change the properties of the Okhotsk Sea intermediate waters and the WSG winter mixed layers, both of which play critical roles in determining the properties of the NPIW and the offshore transport of redox-active trace elements to the North Pacific Ocean.

DATA AVAILABILITY STATEMENT

All datasets generated for this study are included in the manuscript/**Supplementary Files**.

AUTHOR CONTRIBUTIONS

JD, WL, and AS designed the study. PM and MB optimized the sample analysis for dissolved and particulate Mn and Co, and particulate REEs. JS, ED, AM, and AS analyzed the samples for dissolved REEs. PM, JD, WL, JS, ED, and TK performed the data analysis and led the interpretation. PM and JS wrote the first draft of the manuscript. All authors contributed to manuscript revision.

FUNDING

This work was supported by United States NSF OCE 0136977 to JD, United States NSF OCE 0117917 to WL, United States NSF OCE 0137359 to AS, and United States NSF DMR-1644779 and the State of Florida.

SUPPLEMENTARY MATERIAL

The Supplementary Material for this article can be found online at: https://www.frontiersin.org/articles/10.3389/fmars.2019.00591/full#supplementary-material

REFERENCES

Aguilar-Islas, A. M., Hurst, M. P., Buck, K. N., Sohst, B., Smith, G. J., Lohan, M. C., et al. (2007). Micro- and macronutrients in the southeastern Bering Sea: insight into iron-replete and iron-depleted regimes. *Prog. Oceanogr.* 73, 99–126. doi: 10.1016/j.pocean.2006.12.002

Aguilar-Islas, A. M., Rember, R., Nishino, S., Kikuchi, T., and Itoh, M. (2013). Partitioning and lateral transport of iron to the Canada Basin. *Polar Sci.* 7, 82–99. doi: 10.1016/j.polar.2012.11.001

Andreev, A. G. A., and Kusakabe, M. (2001). Interdecadal variability in dissolved oxygen in the intermediate water layer of the Western Subarctic Gyre and

Kuril Basin (Okhotsk Sea). *Geophys. Res. Lett.* 28, 2453–2456. doi: 10.1029/2000GL012688

Bargar, J., Tebo, B., and Villinski, J. (2000). In situ characterization of Mn(II) oxidation by spores of the marine *Bacillus* sp. strain SG-1. *Geochim. Cosmochim. Acta* 64, 2775–2778. doi: 10.1016/S0016-7037(00)00368-9

Bishop, J. K. B., and Fleisher, M. Q. (1987). Particulate manganese dynamics in Gulf Stream warm-core rings and surrounding waters of the N.W. Atlantic. *Geochim. Cosmochim. Acta* 51, 2807–2825. doi: 10.1016/0016-7037(87)90160-8

Bograd, S. J., Thomson, R. E., Rabinovich, A. B., and LeBlond, P. H. (1999). Near-surface circulation of the Northeast Pacific Ocean derived from WOCE-SVP satellite-tracked drifters. *Deep. Res. Part II* 46, 2371–2403. doi: 10.1016/s0967-0645(99)00068-5

Boyle, E. A., Bergquist, B. A., Kayser, R. A., and Mahowald, N. (2005). Iron, manganese, and lead at Hawaii Ocean Time-series station ALOHA: temporal variability and an intermediate water hydrothermal plume. *Geochim. Cosmochim. Acta* 69, 933–952. doi: 10.1016/j.gca.2004.07.034

Breitburg, D., Levin, L. A., Oschlies, A., Grégoire, M., Chavez, F. P., Conley, D. J., et al. (2018). Declining oxygen in the global ocean and coastal waters. *Science* 359:eaam7240. doi: 10.1126/science.aam7240

Brown, M. T., Landing, W. M., and Measures, C. I. (2005). Dissolved and particulate Fe in the western and central North Pacific: results from the 2002 IOC cruise. *Geochem. Geophys. Geosyst.* 6:Q10001. doi: 10.1029/2004GC000893

Buck, C. S., Landing, W. M., and Resing, J. (2013). Pacific Ocean aerosols: deposition and solubility of iron, aluminum, and other trace elements. *Mar. Chem.* 157, 117–130. doi: 10.1016/j.marchem.2013.09.005

Buck, C. S., Landing, W. M., Resing, J. A., and Lebon, G. T. (2006). Aerosol iron and aluminum solubility in the northwest Pacific Ocean: results from the 2002 IOC cruise. *Geochem. Geophys. Geosyst.* 7:Q04M07. doi: 10.1029/2005GC000977

Buck, K. N., Sedwick, P. N., Sohst, B., and Carlson, C. A. (2018). Organic complexation of iron in the eastern tropical South Pacific: results from US GEOTRACES Eastern Pacific Zonal Transect (GEOTRACES cruise GP16). *Mar. Chem.* 201, 229–241. doi: 10.1016/j.marchem.2017.11.007

Buck, K. N., Sohst, B., and Sedwick, P. N. (2015). The organic complexation of dissolved iron along the U.S. GEOTRACES (GA03) North Atlantic Section. *Deep Sea Res. Part II Top. Stud. Oceanogr.* 116, 152–165. doi: 10.1016/j.dsr2.2014.11.016

Burdige, D. J. (1993). The biogeochemistry of manganese and iron reduction in marine sediments. *Earth Sci. Rev.* 35, 249–284. doi: 10.1016/0012-8252(93)90040-e

Burdige, D. J. (2006). *Geochemistry of Marine Sediments*. Princeton, NJ: Princeton University Press.

Chase, Z., Johnson, K. S., Elrod, V. A., Plant, J. N., Fitzwater, S. E., Pickell, L., et al. (2005). Manganese and iron distributions off central California influenced by upwelling and shelf width. *Mar. Chem.* 95, 235–254. doi: 10.1016/j.marchem.2004.09.006

Chen, G., and Wu, J. (2019). Meridional distribution of dissolved manganese in the tropical and Equatorial Pacific. *Geochim. Cosmochim. Acta* 263, 50–67. doi: 10.1016/j.gca.2019.06.048

Chever, F., Rouxel, O. J., Croot, P. L., Ponzevera, E., Wuttig, K., and Auro, M. (2015). Total dissolvable and dissolved iron isotopes in the water column of the Peru upwelling regime. *Geochim. Cosmochim. Acta* 162, 66–82. doi: 10.1016/j.gca.2015.04.031

Chinni, V., Singh, S. K., Bhushan, R., Rengarajan, R., and Sarma, V. V. S. S. (2019). Spatial variability in dissolved iron concentrations in the marginal and open waters of the Indian Ocean. *Mar. Chem.* 208, 11–28. doi: 10.1016/j.marchem.2018.11.007

Cutter, G. A., and Cutter, L. S. (2006). Biogeochemistry of arsenic and antimony in the North Pacific Ocean. *Geochem. Geophys. Geosyst.* 7:12. doi: 10.1029/2005GC001159

Cutter, G. A., Moffett, J. W., Nielsdóttir, M. C., and Sanial, V. (2018). Multiple oxidation state trace elements in suboxic waters off Peru: *in situ* redox processes and advective/diffusive horizontal transport. *Mar. Chem.* 201, 77–89. doi: 10.1016/j.marchem.2018.01.003

de Baar, H. J. W., Bruland, K. W., Schijf, J., van Heuven, S. M. A. C., and Behrens, M. K. (2018). Low cerium among the dissolved rare earth elements in the central North Pacific Ocean. *Geochim. Cosmochim. Acta* 236, 5–40. doi: 10.1016/j.gca.2018.03.003

de Baar, H. J. W., German, C. R., Elderfield, H., and van Gaans, P. (1988). Rare earth element distributions in anoxic waters of the Cariaco Trench. *Geochim. Cosmochim. Acta* 52, 1203–1219. doi: 10.1016/0016-7037(88)90275-X

de Baar, H. J. W. W., Bacon, M. P., Brewer, P. G., and Bruland, K. W. (1985). Rare earth elements in the Pacific and Atlantic Oceans. *Geochim. Cosmochim. Acta* 49, 1943–1959. doi: 10.1016/0016-7037(85)90089-4

De Carlo, E. H., Wen, X.-Y., and Irving, M. (1997). The influence of redox reactions on the uptake of dissolved Ce by suspended Fe and Mn oxide particles. *Aquat. Geochem.* 3, 357–389. doi: 10.1023/A:1009664626181

Dick, G. J., Podell, S., Johnson, H. A., Rivera-Espinoza, Y., Bernier-Latmani, R., McCarthy, J. K., et al. (2008). Genomic insights into Mn(II) oxidation by the marine alphaproteobacterium Aurantimonas sp. strain SI85-9A1. *Appl. Environ. Microbiol.* 74, 2646–2658. doi: 10.1128/AEM.01656-07

Dulaquais, G., Boye, M., Middag, R., Owens, S., Puigcorbe, V., Buesseler, K., et al. (2014). Contrasting biogeochemical cycles of cobalt in the surface western Atlantic Ocean. *Glob. Biogeochem. Cycles* 28, 1387–1412. doi: 10.1002/2014GB004903

Eggimann, D., and Betzer, P. (1976). Decomposition and analysis of refractory oceanic suspended materials. *Anal. Chem.* 48, 886–890. doi: 10.1021/ac60370a005

Eggins, S. M., Woodhead, J. D., Kinsley, L. P. J., Mortimer, G. E., Sylvester, P., McCulloch, M. T., et al. (1997). A simple method for the precise determination of = 40 trace elements in geological samples by ICPMS using enriched isotope internal standardisation. *Chem. Geol.* 134, 311–326. doi: 10.1016/S0009-2541(96)00100-3

Elderfield, H. (1988). The oceanic chemistry of the rare-earth elements and discussion. *Philos. Trans. R. Soc. A Math. Phys. Eng. Sci.* 325, 105–126. doi: 10.1098/rsta.1988.0046

Ellwood, M. J., and van den Berg, C. M. (2001). Determination of organic complexation of cobalt in seawater by cathodic stripping voltammetry. *Mar. Chem.* 75, 33–47. doi: 10.1016/S0304-4203(01)00024-X

Elrod, V. A., Berelson, W. M., Coale, K. H., and Johnson, K. S. (2004). The flux of iron from continental shelf sediments: a missing source for global budgets. *Geophys. Res. Lett.* 31:L12307. doi: 10.1029/2004GL020216

Ezoe, M., Ishita, T., Kinugasa, M., Lai, X., Norisuye, K., and Sohrin, Y. (2004). Distributions of dissolved and acid-dissolvable bioactive trace metals in the North Pacific Ocean. *Geochem. J.* 38, 535–550. doi: 10.2343/geochemj.38.535

Fitzsimmons, J. N., Carrasco, G. G., Wu, J., Roshan, S., Hatta, M., Measures, C. I., et al. (2015a). Partitioning of dissolved iron and iron isotopes into soluble and colloidal phases along the GA03 GEOTRACES North Atlantic Transect. *Deep Sea Res. Part II Top. Stud. Oceanogr.* 116, 130–151. doi: 10.1016/j.dsr2.2014.11.014

Fitzsimmons, J. N., Hayes, C. T., Al-Subiai, S. N., Zhang, R., Morton, P. L., Weisend, R. E., et al. (2015b). Daily to decadal variability of size-fractionated iron and iron-binding ligands at the Hawaii Ocean time-series station ALOHA. *Geochim. Cosmochim. Acta* 171, 303–324. doi: 10.1016/j.gca.2015.08.012

Fröllje, H., Pahnke, K., Schnetger, B., Brumsack, H.-J., Dulai, H., and Fitzsimmons, J. N. (2016). Hawaiian imprint on dissolved Nd and Ra isotopes and rare earth elements in the central North Pacific: local survey and seasonal variability. *Geochim. Cosmochim. Acta* 189, 110–131. doi: 10.1016/j.gca.2016.06.001

Fujishima, Y., Ueda, K., Maruo, M., Nakayama, E., Tokutome, C., Hasegawa, H., et al. (2001). Distribution of trace bioelements in the Subarctic North Pacific Ocean and the Bering Sea (the R/V Hakuho Maru Cruise KH-97-2). *J. Oceanogr.* 57, 261–273. doi: 10.1023/A:1012426411228

Gallon, C., Ranville, M. A. M. A., Conaway, C. H. C. H., Landing, W. M. W. M., Buck, C. S. C. S., Morton, P. L. P. L., et al. (2011). Asian industrial lead inputs to the North Pacific evidenced by lead concentrations and isotopic compositions in surface waters and aerosols. *Environ. Sci. Technol.* 45, 9874–9882. doi: 10.1021/es2020428

GeoReM, (2009). *Geological and Environmental Reference Materials*. Available at: georem.mpch-mainz.gwdg.de/ (accessed August 16, 2019).

German, C. R., and Elderfield, H. (1990). Rare earth elements in the NW Indian Ocean. *Geochim. Cosmochim. Acta* 54, 1929–1940. doi: 10.1016/0016-7037(90)90262-J

Glass, J. B. J. B., Kretz, C. B. C. B., Ganesh, S., Ranjan, P., Seston, S. L. S. L., Buck, K. N. K. N., et al. (2015). Meta-omic signatures of microbial metal and nitrogen cycling in marine oxygen minimum zones. *Front. Microbiol.* 6:998. doi: 10.3389/fmicb.2015.00998

Grand, M. M., Measures, C. I., Hatta, M., Hiscock, W. T., Buck, C. S., and Landing, W. M. (2015a). Dust deposition in the eastern Indian Ocean: the ocean perspective from Antarctica to the Bay of Bengal. *Glob. Biogeochem. Cycles* 29, 357–374. doi: 10.1002/2014GB004898

Grand, M. M., Measures, C. I., Hatta, M., Morton, P. L., Barrett, P., Milne, A., et al. (2015b). The impact of circulation and dust deposition in controlling the distributions of dissolved Fe and Al in the south Indian subtropical gyre. *Mar. Chem.* 176, 110–125. doi: 10.1016/j.marchem.2015.08.002

Grenier, M., Jeandel, C., Lacan, F., Vance, D., Venchiarutti, C., Cros, A., et al. (2013). From the subtropics to the central equatorial Pacific Ocean: neodymium isotopic composition and rare earth element concentration variations. *J. Geophys. Res. Ocean* 118, 592–618. doi: 10.1029/2012JC008239

Hammerschmidt, C. R., and Bowman, K. L. (2012). Vertical methylmercury distribution in the subtropical North Pacific Ocean. *Mar. Chem.* 132–133, 77–82. doi: 10.1016/j.marchem.2012.02.005

Hansel, C. M. (2017). Manganese in marine microbiology. *Adv. Microb. Physiol.* 70, 37–83. doi: 10.1016/bs.ampbs.2017.01.005

Hansell, D. A., Carlson, C. A., and Suzuki, Y. (2002). Dissolved organic carbon export with North Pacific intermediate water formation. *Glob. Biogeochem. Cycles* 16, 7–1. doi: 10.1029/2000GB001361

Hathorne, E. C., Haley, B., Stichel, T., Grasse, P., Zieringer, M., and Frank, M. (2012). Online preconcentration ICP-MS analysis of rare earth elements in seawater. *Geochem. Geophys. Geosyst.* 13, 1–12. doi: 10.1029/2011GC003907

Hatta, M., Measures, C. I., Wu, J., Roshan, S., Fitzsimmons, J. N., Sedwick, P., et al. (2015). An overview of dissolved Fe and Mn distributions during the 2010–2011 U.S. GEOTRACES north Atlantic cruises: GEOTRACES GA03. *Deep Sea Res. Part II Top. Stud. Oceanogr.* 116, 117–129. doi: 10.1016/j.dsr2.2014.07.005

Hawco, N. J., Lam, P. J., Lee, J.-M., Ohnemus, D. C., Noble, A. E., Wyatt, N. J., et al. (2018). Cobalt scavenging in the mesopelagic ocean and its influence on global mass balance: synthesizing water column and sedimentary fluxes. *Mar. Chem.* 201, 151–166. doi: 10.1016/j.marchem.2017.09.001

Hawco, N. J., Ohnemus, D. C., Resing, J. A., Twining, B. S., and Saito, M. A. (2016). A dissolved cobalt plume in the oxygen minimum zone of the eastern tropical South Pacific. *Biogeosciences* 13, 5697–5717. doi: 10.5194/bg-13-5697-2016

Heller, M. I., Lam, P. J., Moffett, J. W., Till, C. P., Lee, J.-M., Toner, B. M., et al. (2017). Accumulation of Fe oxyhydroxides in the Peruvian oxygen deficient zone implies non-oxygen dependent Fe oxidation. *Geochim. Cosmochim. Acta* 211, 174–193. doi: 10.1016/j.gca.2017.05.019

Hernes, P. J., and Benner, R. (2002). Transport and diagenesis of dissolved and particulate terrigenous organic matter in the North Pacific Ocean. *Deep Sea Res. Part I Oceanogr. Res. Pap.* 49, 2119–2132. doi: 10.1016/S0967-0637(02)00128-0

Hsu, S.-C., Liu, S. C., Huang, Y.-T., Lung, S.-C. C., Tsai, F., Tu, J.-Y., et al. (2008). A criterion for identifying Asian dust events based on Al concentration data collected from northern Taiwan between 2002 and early 2007. *J. Geophys. Res.* 113:D18306. doi: 10.1029/2007JD009574

Hsu, S.-C., Wong, G. T. F., Gong, G.-C., Shiah, F.-K., Huang, Y.-T., Kao, S.-J., et al. (2010). Sources, solubility, and dry deposition of aerosol trace elements over the East China Sea. *Mar. Chem.* 120, 116–127. doi: 10.1016/j.marchem.2008.10.003

Jacobs, L., Emerson, S., and Huested, S. S. (1987). Trace metal geochemistry in the Cariaco Trench. *Deep Sea Res. Part A Oceanogr. Res. Pap.* 34, 965–981. doi: 10.1016/0198-0149(87)90048-3

Jickells, T. D., An, Z. S., Andersen, K. K., Baker, A. R., Bergametti, G., Brooks, N., et al. (2005). Global iron connections between desert dust, ocean biogeochemistry, and climate. *Science* 308, 67–71. doi: 10.1126/science.1105959

Johnson, K. K. S., Coale, K. K. H., Berelson, W. W. M., Gordon, R., and Michael Gordon, R. (1996). On the formation of the manganese maximum in the oxygen minimum. *Geochim. Cosmochim. Acta* 60, 1291–1299. doi: 10.1016/0016-7037(96)00005-1

Kim, W., Doh, S.-J., and Yu, Y. (2012). Asian dust storm as conveyance media of anthropogenic pollutants. *Atmos. Environ.* 49, 41–50. doi: 10.1016/J.ATMOSENV.2011.12.034

Kinugasa, M., Ishita, T., Sohrin, Y., Okamura, K., Takeda, S., Nishioka, J., et al. (2005). Dynamics of trace metals during the subarctic Pacific iron experiment for ecosystem dynamics study (SEEDS2001). *Prog. Oceanogr.* 64, 129–147. doi: 10.1016/j.pocean.2005.02.005

Klar, J. K., Schlosser, C., Milton, J. A., Woodward, E. M. S., Lacan, F., Parkinson, I. J., et al. (2018). Sources of dissolved iron to oxygen minimum zone waters on the Senegalese continental margin in the tropical North Atlantic Ocean: insights from iron isotopes. *Geochim. Cosmochim. Acta* 236, 60–78. doi: 10.1016/j.gca.2018.02.031

Klunder, M. B., Laan, P., De Baar, H. J. W., Middag, R., Neven, I., and Van Ooijen, J. (2014). Dissolved Fe across the Weddell Sea and Drake passage: impact of DFe on nutrient uptake. *Biogeosciences* 11, 651–669. doi: 10.5194/bg-11-651-2014

Knauer, G. A., Martin, J. H., and Gordon, R. M. (1982). Cobalt in north-east Pacific waters. *Nature* 297, 49–51. doi: 10.1038/297049a0

Kondo, Y., and Moffett, J. W. (2013). Dissolved Fe(II) in the Arabian Sea oxygen minimum zone and western tropical Indian Ocean during the inter-monsoon period. *Deep Sea Res. Part I Oceanogr. Res. Pap.* 73, 73–83. doi: 10.1016/j.dsr.2012.11.014

Kondo, Y., and Moffett, J. W. (2015). Iron redox cycling and subsurface offshore transport in the eastern tropical South Pacific oxygen minimum zone. *Mar. Chem.* 168, 95–103. doi: 10.1016/j.marchem.2014.11.007

Lam, P. J., and Bishop, J. K. B. (2008). The continental margin is a key source of iron to the HNLC North Pacific Ocean. *Geophys. Res. Lett.* 35:L07608. doi: 10.1029/2008GL033294

Lam, P. J., Bishop, J. K. B., Henning, C. C., Marcus, M. A., Waychunas, G. A., and Fung, I. Y. (2006). Wintertime phytoplankton bloom in the subarctic Pacific supported by continental margin iron. *Glob. Biogeochem. Cycles* 20:GB2006. doi: 10.1029/2005GB002557

Lam, P. J., Ohnemus, D. C., and Auro, M. E. (2015). Size-fractionated major particle composition and concentrations from the US GEOTRACES North Atlantic Zonal Transect. *Deep Sea Res. Part II Top. Stud. Oceanogr.* 116, 303–320. doi: 10.1016/j.dsr2.2014.11.020

Lamborg, C. H., Buesseler, K. O., and Lam, P. J. (2008). Sinking fluxes of minor and trace elements in the North Pacific Ocean measured during the VERTIGO program. *Deep Sea Res. Part II Top. Stud. Oceanogr.* 55, 1564–1577. doi: 10.1016/j.dsr2.2008.04.012

Landing, W. M., and Bruland, K. W. (1980). Manganese in the North Pacific. *Earth Planet. Sci. Lett.* 49, 45–56.

Landing, W. M., and Bruland, K. W. (1987). The contrasting biogeochemistry of iron and manganese in the Pacific Ocean. *Geochim. Cosmochim. Acta* 51, 29–43. doi: 10.1016/0016-7037(87)90004-4

Laurier, F. J. G., Mason, R. P., Gill, G. A., and Whalin, L. (2004). Mercury distributions in the North Pacific Ocean—20 years of observations. *Mar. Chem.* 90, 3–19. doi: 10.1016/j.marchem.2004.02.025

Learman, D. R., Wankel, S. D., Webb, S. M., Martinez, N., Madden, A. S., and Hansel, C. M. (2011). Coupled biotic–abiotic Mn(II) oxidation pathway mediates the formation and structural evolution of biogenic Mn oxides. *Geochim. Cosmochim. Acta* 75, 6048–6063. doi: 10.1016/j.gca.2011.07.026

Lewis, B. L., and Landing, W. M. (1991). The biogeochemistry of manganese and iron in the Black Sea. *Deep Sea Res. Part A Oceanogr. Res. Pap.* 38, S773–S803. doi: 10.1016/S0198-0149(10)80009-3

Lewis, B. L., and Luther, G. W. (2000). Processes controlling the distribution and cycling of manganese in the oxygen minimum zone of the Arabian Sea. *Deep. Res. Part II Top. Stud. Oceanogr.* 47, 1541–1561. doi: 10.1016/S0967-0645(99)00153-8

Lin, I. I., Chen, J. P., Wong, G. T. F., Huang, C. W., and Lien, C. C. (2007). Aerosol input to the South China Sea: results from the MODerate resolution imaging spectro-radiometer, the quick scatterometer, and the measurements of pollution in the troposphere sensor. *Deep. Res. Part II* 54, 1589–1601. doi: 10.1016/j.dsr2.2007.05.013

Mahowald, N. M., Baker, A. R., Bergametti, G., Brooks, N., Duce, R. A., Jickells, T. D., et al. (2005). Atmospheric global dust cycle and iron inputs to the ocean. *Glob. Biogeochem. Cycles* 19:GB4025. doi: 10.1029/2004GB002402

Mahowald, N. M., Engelstaedter, S., Luo, C., Sealy, A., Artaxo, P., Benitez-Nelson, C., et al. (2009). Atmospheric iron deposition: global distribution, variability, and human perturbations. *Ann. Rev. Mar. Sci.* 1, 245–278. doi: 10.1146/annurev.marine.010908.163727

Marsay, C. M., Lam, P. J., Heller, M. I., Lee, J.-M., and John, S. G. (2018). Distribution and isotopic signature of ligand-leachable particulate iron along the GEOTRACES GP16 East Pacific Zonal Transect. *Mar. Chem.* 201, 198–211. doi: 10.1016/j.marchem.2017.07.003

Martin, J. H., Knauer, G. A., and Broenkow, W. W. (1985). VERTEX: the lateral transport of manganese in the northeast Pacific. *Deep Sea Res. Part A Oceanogr. Res. Pap.* 32, 1405–1412,1414–1427.

Measures, C. I., Brown, M. T., and Vink, S. (2005). Dust deposition to the surface waters of the Western and Central North Pacific inferred from surface water dissolved aluminum concentrations. *Geochem. Geophys. Geosyst.* 6:Q09M03. doi: 10.1029/2005GC000922

Measures, C. I., Cutter, G. A., Landing, W. M., and Powell, R. T. (2006). Hydrographic observations during the 2002 IOC contaminant baseline survey in the western Pacific Ocean. *Geochem. Geophys. Geosyst.* 7, 1–14. doi: 10.1029/2004GC000855

Middag, R., de Baar, H. J. W., Klunder, M. B., and Laan, P. (2013). Fluxes of dissolved aluminum and manganese to the Weddell Sea and indications for manganese co-limitation. *Limnol. Oceanogr.* 58, 287–300. doi: 10.4319/lo.2013.58.1.0287

Middag, R., de Baar, H. J. W., Laan, P., Cai, P. H., and van Ooijen, J. C. (2011a). Dissolved manganese in the Atlantic sector of the Southern Ocean. *Deep Sea Res. Part II Top. Stud. Oceanogr.* 58, 2661–2677. doi: 10.1016/j.dsr2.2010.10.043

Middag, R., de Baar, H. J. W., Laan, P., and Klunder, M. B. (2011b). Fluvial and hydrothermal input of manganese into the Arctic Ocean. *Geochim. Cosmochim. Acta* 75, 2393–2408. doi: 10.1016/j.gca.2011.02.011

Middag, R., de Baar, H. J. W., Laan, P., and Huhn, O. (2012). The effects of continental margins and water mass circulation on the distribution of dissolved aluminum and manganese in Drake Passage. *J. Geophys. Res. Ocean* 117:C01019. doi: 10.1029/2011JC007434

Middag, R., Séférian, R., Conway, T. M., John, S. G., Bruland, K. W., and de Baar, H. J. W. (2015). Intercomparison of dissolved trace elements at the Bermuda Atlantic Time Series station. *Mar. Chem.* 177, 476–489. doi: 10.1016/J.MARCHEM.2015.06.014

Milne, A., Landing, W. M., Bizimis, M., and Morton, P. L. (2010). Determination of Mn, Fe, Co, Ni, Cu, Zn, Cd and Pb in seawater using high resolution magnetic sector inductively coupled mass spectrometry (HR-ICP-MS). *Anal. Chim. Acta* 665, 200–207. doi: 10.1016/j.aca.2010.03.027

Minakawa, M., Noriki, S., and Tsunogai, S. (1996). Manganese in the East China Sea and the Yellow Sea. *Geochem. J.* 30, 41–55. doi: 10.2343/geochemj.30.41

Misumi, K., Tsumune, D., Yoshida, Y., Uchimoto, K., Nakamura, T., Nishioka, J., et al. (2011). Mechanisms controlling dissolved iron distribution in the North Pacific: a model study. *J. Geophys. Res. Biogeosci.* 116:G03005. doi: 10.1029/2010JG001541

Mitsudera, H., Taguchi, B., Yoshikawa, Y., Nakamura, H., Waseda, T., and Qu, T. (2004). Numerical study on the Oyashio water pathways in the Kuroshio–Oyashio confluence. *J. Phys. Oceanogr.* 34, 1174–1196. doi: 10.1175/1520-0485(2004)034<1174:nsotow>2.0.co;2

Moffett, J. W. (1990). Microbially mediated cerium oxidation in sea water. *Nature* 345, 421–423. doi: 10.1038/345421a0

Moffett, J. W. (1994a). A radiotracer study of cerium and manganese uptake onto suspended particles in Chesapeake Bay. *Geochim. Cosmochim. Acta* 58, 695–703. doi: 10.1016/0016-7037(94)90499-5

Moffett, J. W. (1994b). The relationship between cerium and manganese oxidation in the marine environment. *Limnol. Oceanogr.* 39, 1309–1318. doi: 10.4319/lo.1994.39.6.1309

Moffett, J. W. (1997). The importance of microbial Mn oxidation in the upper ocean: a comparison of the Sargasso Sea and equatorial Pacific. *Deep Res. Part I* 44, 1277–1291. doi: 10.1016/s0967-0637(97)00032-0

Moffett, J. W., and Ho, J. (1996). Oxidation of cobalt and manganese in seawater via a common microbially catalyzed pathway. *Geochim. Cosmochim. Acta* 60, 3415–3424. doi: 10.1016/0016-7037(96)00176-7

Morel, F. M. M., Milligan, A. J., and Saito, M. A. (2003). "Marine bioinorganic chemistry: the role of trace metals in the oceanic cycles of major nutrients," in *Treatise on Geochemistry*, eds H. Elderfield, H. D. Holland, and K. K. Turekian, (Cambridge: Elsevier Science Ltd.), 113–143. doi: 10.1016/b0-08-043751-6/06108-9

Murray, K. J., Webb, S. M., Bargar, J. R., and Tebo, B. M. (2007). Indirect oxidation of Co(II) in the presence of the marine Mn(II)-oxidizing bacterium Bacillus sp. strain SG-1. *Appl. Environ. Microbiol.* 73, 6905–6909. doi: 10.1128/aem.00971-07

Nakatsuka, T., Fujimune, T., Yoshikawa, C., Noriki, S., Kawamura, K., Fukamachi, Y., et al. (2004a). Biogenic and lithogenic particle fluxes in the western region of the Sea of Okhotsk: implications for lateral material transport and biological productivity. *J. Geophys. Res.* 109:C09S13. doi: 10.1029/2003JC001908

Nakatsuka, T., Toda, M., Kawamura, K., and Wakatsuchi, M. (2004b). Dissolved and particulate organic carbon in the Sea of Okhotsk: transport from continental shelf to ocean interior. *J. Geophys. Res.* 109:C09S14.

Nishioka, J., and Obata, H. (2017). Dissolved iron distribution in the western and central subarctic Pacific: HNLC water formation and biogeochemical processes. *Limnol. Oceanogr.* 62, 2004–2022. doi: 10.1002/LNO.10548

Nishioka, J., Ono, T., Saito, H., Nakatsuka, T., Takeda, S., Yoshimura, T., et al. (2007). Iron supply to the Western Subarctic Pacific: importance of iron export from the Sea of Okhotsk. *J. Geophys. Res.* 112:C10012. doi: 10.1029/2006JC004055

Noble, A. E., Lamborg, C. H., Ohnemus, D. C., Lam, P. J., Goepfert, T. J., Measures, C. I., et al. (2012). Basin-scale inputs of cobalt, iron, and manganese from the Benguela-Angola front to the South Atlantic Ocean. *Limnol. Oceanogr.* 57, 989–1010. doi: 10.4319/lo.2012.57.4.0989

Noble, A. E., Ohnemus, D. C., Hawco, N. J., Lam, P. J., and Saito, M. A. (2017). Coastal sources, sinks and strong organic complexation of dissolved cobalt within the US North Atlantic GEOTRACES transect GA03. *Biogeosciences* 14, 2715–2739. doi: 10.5194/bg-14-2715-2017

Noble, A. E., Saito, M. A., Maiti, K., and Benitez-Nelson, C. R. (2008). Cobalt, manganese, and iron near the Hawaiian Islands: a potential concentrating mechanism for cobalt within a cyclonic eddy and implications for the hybrid-type trace metals. *Deep Sea Res. Part II Top. Stud. Oceanogr.* 55, 1473–1490. doi: 10.1016/j.dsr2.2008.02.010

Noffke, A., Hensen, C., Sommer, S., Scholz, F., Bohlen, L., Mosch, T., et al. (2012). Benthic iron and phosphorus fluxes across the Peruvian oxygen minimum zone. *Limnol. Oceanogr.* 57, 851–867. doi: 10.4319/lo.2012.57.3.0851

Noriki, S., Shimizu, M., Hamahara, K., Narita, H., Saino, T., and Yanagi, T. (1997). Transportation of particulate material through the mouth of Tokyo Bay to the open ocean. *J. Oceanogr.* 53, 571–578.

Nozaki, Y. (2001). "Rare earth elements and their isotopes in the ocean," in *Encyclopedia of Ocean Sciences*, eds J. H. Steele, S. A. Thorpe, and K. K. Turekian (Amsterdam: Elsevier), 653–665. doi: 10.1016/B978-012374473-9.00284-8

Obata, H., Alibo, D. S., and Nozaki, Y. (2007). Dissolved aluminum, indium, and cerium in the Sea of Japan and the Sea of Okhotsk: comparison to the marginal seas of the western North Pacific. *J. Geophys. Res.* 112:C12003. doi: 10.1029/2006jc003944

Ohnemus, D. C., Auro, M. E., Sherrell, R. M., Lagerström, M., Morton, P. L., Twining, B. S., et al. (2014). Laboratory intercomparison of marine particulate digestions including Piranha: a novel chemical method for dissolution of polyethersulfone filters. *Limnol. Oceanogr. Methods* 12, 530–547. doi: 10.4319/lom.2014.12.530

Ohshima, K., Wakatsuchi, M., and Saitoh, S.-I. (2005). Velocity field of the Oyashio region observed with satellite-tracked surface drifters during 1999–2000. *J. Oceanogr.* 61, 845–855. doi: 10.1007/s10872-006-0004-3

Oka, E., and Qiu, B. (2012). Progress of North Pacific mode water research in the past decade. *J. Oceanogr.* 68, 5–20. doi: 10.1007/s10872-011-0032-5

Oka, E., and Suga, T. (2005). Differential formation and circulation of North Pacific Central mode water. *J. Phys. Oceanogr.* 35, 1997–2011. doi: 10.1175/jpo2811.1

Oka, E., Suga, T., Sukigara, C., Toyama, K., Shimada, K., and Yoshida, J. (2011). "Eddy resolving" observation of the North Pacific subtropical mode water. *J. Phys. Oceanogr.* 41, 666–681. doi: 10.1175/2011JPO4501.1

Oka, E., Talley, L. D., and Suga, T. (2007). Temporal variability of winter mixed layer in the mid-to high-latitude North Pacific. *J. Oceanogr.* 63, 293–307. doi: 10.1007/s10872-007-0029-2

Oka, E., Toyama, K., and Suga, T. (2009). Subduction of North Pacific central mode water associated with subsurface mesoscale eddy. *Geophys. Res. Lett.* 36:L08607. doi: 10.1029/2009GL037540

Okin, G. S., Baker, A. R., Tegen, I., Mahowald, N. M., Dentener, F. J., Duce, R. A., et al. (2011). Impacts of atmospheric nutrient deposition on marine productivity: roles of nitrogen, phosphorus, and iron. *Glob. Biogeochem. Cycles* 25:GB2022.

Okubo, A., Takeda, S., and Obata, H. (2013). Atmospheric deposition of trace metals to the western North Pacific Ocean observed at coastal station in Japan. *Atmos. Res.* 129–130, 20–32. doi: 10.1016/j.atmosres.2013.03.014

Oldham, V. E., Jones, M. R., Tebo, B. M., and Luther, G. W. (2017). Oxidative and reductive processes contributing to manganese cycling at oxic-anoxic interfaces. *Mar. Chem.* 195, 122–128. doi: 10.1016/J.MARCHEM.2017.06.002

Otosaka, S., and Noriki, S. (2000). REEs and Mn/Al ratio of settling particles: horizontal transport of particulate material in the northern Japan Trench. *Mar. Chem.* 72, 329–342. doi: 10.1016/s0304-4203(00)00094-3

Pahnke, K., van de Flierdt, T., Jones, K. M., Lambelet, M., Hemming, S. R., and Goldstein, S. L. (2012). GEOTRACES intercalibration of neodymium isotopes and rare earth element concentrations in seawater and suspended particles. Part 2: systematic tests and baseline profiles. *Limnol. Oceanogr. Methods* 10, 252–269. doi: 10.4319/lom.2012.10.252

Paik, S., Min, S.-K., Kim, Y.-H., Kim, B.-M., Shiogama, H., and Heo, J. (2017). Attributing causes of 2015 record minimum sea-ice extent in the Sea of Okhotsk. *J. Clim.* 30, 4693–4703. doi: 10.1175/JCLI-D-16-0587.1

Paulmier, A., and Ruiz-Pino, D. (2009). Oxygen minimum zones (OMZs) in the modern ocean. *Prog. Oceanogr.* 80, 113–128. doi: 10.1016/j.pocean.2008.08.001

Qiu, B. (1995). Why is the spreading of the north Pacific intermediate water confined on density surfaces around σθ = 26.8?. *J. Phys. Oceanogr.* 25, 168–180. doi: 10.1175/1520-04851995025<0168:witsot<2.0.co;2

Qiu, B., and Chen, S. (2005). Variability of the Kuroshio extension jet, recirculation gyre, and mesoscale eddies on decadal time scales. *J. Phys. Oceanogr.* 35, 2090–2103. doi: 10.1175/jpo2807.1

Ranville, M. A., Cutter, G. A., Buck, C. S., Landing, W. M., Cutter, L. S., Resing, J. A., et al. (2010). Aeolian contamination of Se and Ag in the North Pacific from Asian fossil fuel combustion. *Environ. Sci. Technol.* 44, 1587–1593. doi: 10.1021/es902523m

Ranville, M. A., and Flegal, A. R. (2005). Silver in the North Pacific Ocean. *Geochem. Geophys. Geosyst.* 6:Q03M01.

Rudnick, R. L., and Gao, S. (2003). Composition of the continental crust. *Treatise Geochem.* 3, 1–64. doi: 10.1016/B0-08-043751-6/03016-4

Saager, P. M., De Baar, H. J. W., and Burkill, P. H. (1989). Manganese and iron in Indian Ocean waters. *Geochim. Cosmochim. Acta* 53, 2259–2267. doi: 10.1016/0016-7037(89)90348-7

Saito, M. A., and Moffett, J. W. (2001). Complexation of cobalt by natural organic ligands in the Sargasso Sea as determined by a new high-sensitivity electrochemical cobalt speciation method suitable for open ocean work. *Mar. Chem.* 75, 49–68. doi: 10.1016/s0304-4203(01)00025-1

Saito, M. A., and Moffett, J. W. (2002). Temporal and spatial variability of cobalt in the Atlantic Ocean. *Geochim. Cosmochim. Acta* 66, 1943–1953. doi: 10.1016/s0016-7037(02)00829-3

Saito, M. A., Moffett, J. W., and DiTullio, G. R. (2004). Cobalt and nickel in the Peru upwelling region: a major flux of labile cobalt utilized as a micronutrient. *Glob. Biogeochem. Cycles* 18:GB4030. doi: 10.1029/2003GB002216

Saito, M. A., Rocap, G., and Moffett, J. W. (2005). Production of cobalt binding ligands in a Synechococcus feature at the Costa Rica upwelling dome. *Limnol. Oceanogr.* 50, 279–290. doi: 10.4319/lo.2005.50.1.0279

Schijf, J., Christenson, E. A., and Byrne, R. H. (2015). YREE scavenging in seawater: a new look at an old model. *Mar. Chem.* 177, 460–471. doi: 10.1016/j.marchem.2015.06.010

Scholz, F. (2018). Identifying oxygen minimum zone-type biogeochemical cycling in Earth history using inorganic geochemical proxies. *Earth Sci. Rev.* 184, 29–45. doi: 10.1016/j.earscirev.2018.08.002

Sedwick, P., Sohst, B. M., Ussher, S. J., and Bowie, A. R. (2015). A zonal picture of the water column distribution of dissolved iron(II) during the U.S. GEOTRACES North Atlantic transect cruise (GEOTRACES GA03). *Deep Sea Res. Part II Top. Stud. Oceanogr.* 116, 166–175. doi: 10.1016/j.dsr2.2014.11.004

Shcherbina, A. Y., Talley, L. D., and Rudnick, D. L. (2004). Dense water formation on the northwestern shelf of the Okhotsk Sea: 2. Quantifying the transports. *J. Geophys. Res.* 109:C09S09. doi: 10.1029/2003JC002197

Sherrell, R. M., Annett, A. L., Fitzsimmons, J. N., Roccanova, V. J., and Meredith, M. P. (2018). A "shallow bathtub ring" of local sedimentary iron input maintains the Palmer Deep biological hotspot on the West Antarctic Peninsula shelf. *Philos. Trans. A. Math. Phys. Eng. Sci.* 376:20170171. doi: 10.1098/rsta.2017.0171

Shiller, A. M. (1997). Manganese in surface waters of the Atlantic Ocean. *Geophys. Res. Lett.* 24, 1495–1498. doi: 10.1029/97GL01456

Shiller, A. M., and Bairamadgi, G. R. (2006). Dissolved gallium in the Northwest Pacific and the South and Central Atlantic Oceans: implications for aeolian Fe input and a reconsideration of profiles. *Geochem. Geophys. Geosyst.* 7:Q08M09. doi: 10.1029/2005GC001118

Spiro, T. G., Bargar, J. R., Sposito, G., and Tebo, B. M. (2010). Bacteriogenic manganese oxides. *Acc. Chem. Res.* 43, 2–9. doi: 10.1021/ar800232a

Stumm, W., and Morgan, J. J. (1995). *Aquatic Chemistry: Chemical Equilibria and Rates in Natural Waters*, 3rd Edn. New York, NY: Wiley.

Sunda, W. G. (2012). Feedback interactions between trace metal nutrients and phytoplankton in the ocean. *Front. Microbiol.* 3:204. doi: 10.3389/fmicb.2012.00204

Sunda, W. G., and Huntsman, S. A. (1988). Effect of sunlight on redox cycles of manganese in the southwestern Sargasso Sea. *Deep Sea Res. Part A Oceanogr. Res. Pap.* 35, 1297–1317. doi: 10.1016/0198-0149(88)90084-2

Sunda, W. G., and Huntsman, S. A. (1994). Photoreduction of manganese oxides in seawater. *Mar. Chem.* 46, 133–152. doi: 10.1016/0304-4203(94)90051-5

Sunda, W. G., and Huntsman, S. A. (1996). Antagonisms between cadmium and zinc toxicity and manganese limitation in a coastal diatom. *Limnol. Oceanogr.* 41, 373–387. doi: 10.4319/lo.1996.41.3.0373

Sunda, W. G., and Huntsman, S. A. (2000). Effect of Zn, Mn, and Fe on Cd accumulation in phytoplankton: implications for oceanic Cd cycling. *Limnol. Oceanogr.* 45, 1501–1516. doi: 10.4319/lo.2000.45.7.1501

Sunda, W. G., Huntsman, S. A., and Harvey, G. R. (1983). Photoreduction of manganese oxides in seawater and its geochemical and biological implications. *Nature* 301, 234–236. doi: 10.1038/301234a0

Sundby, B., Anderson, L. G., Hall, P. O. J., Iverfeldt, A., Rutgers van der Loeff, M. M., and Westerlund, S. F. G. (1986). The effect of oxygen on release and uptake of cobalt, manganese, iron and phosphate at the sediment-water interface. *Geochim. Cosmochim. Acta* 50, 1281–1288. doi: 10.1016/0016-7037(86)90411-4

Tachikawa, K., Jeandel, C., Vangriesheim, A., and Dupré, B. (1999). Distribution of rare earth elements and neodymium isotopes in suspended particles of the tropical Atlantic Ocean (EUMELI site). *Deep. Res. Part I* 46, 733–755. doi: 10.1016/s0967-0637(98)00089-2

Tagliabue, A., Bowie, A. R., Boyd, P. W., Buck, K. N., Johnson, K. S., and Saito, M. A. (2017). The integral role of iron in ocean biogeochemistry. *Nature* 543, 51–59. doi: 10.1038/nature21058

Tagliabue, A., Hawco, N. J., Bundy, R. M., Landing, W. M., Milne, A., Morton, P. L., et al. (2018). The role of external inputs and internal cycling in shaping the global ocean cobalt distribution: insights from the first cobalt biogeochemical model. *Global Biogeochem. Cycles* 32, 594–616. doi: 10.1002/2017GB005830

Takeda, S., Obata, H., Okubo, A., Sato, M., and Kondo, Y. (2014). "Bioavailability and biogeochemical processes of trace metals in the surface ocean," in *Western Pacific Air-Sea Interaction Study*, eds M. Uematsu, Y. Yokouchi, Y. W. Watanabe, S. Takeda, and Y. Yamanaka, (Tokyo: TERRAPUB), 163–176. doi: 10.5047/w-pass.a03.001

Talley, L. D., Nagata, Y., Fujimura, M., Iwao, T., Kono, T., Inagake, D., et al. (1995). North Pacific Intermediate Water in the Kuroshio/Oyashio mixed water region. *J. Phys. Oceanogr.* 25, 475–501. doi: 10.1175/1520-04851995025<0475:NPIWIT<2.0.CO;2

Talley, L. D., and Yun, J.-Y. (2001). The role of cabbeling and double diffusion in setting the density of the North Pacific intermediate water salinity minimum. *J. Phys. Oceanogr.* 31, 1538–1549. doi: 10.1175/1520-0485(2001)031<1538:trocad>2.0.co;2

Tanaka, T., Yasuda, I., Kuma, K., and Nishioka, J. (2012). Vertical turbulent iron flux sustains the Green Belt along the shelf break in the southeastern Bering Sea. *Geophys. Res. Lett.* 39:L08603. doi: 10.1029/2012GL051164

Tani, H., Nishioka, J., Kuma, K., Takata, H., Yamashita, Y., Tanoue, E., et al. (2003). Iron (III) hydroxide solubility and humic-type fluorescent organic matter in the deep water column of the Okhotsk Sea and the northwestern North Pacific Ocean. *Deep. Res. Part I* 50, 1063–1078. doi: 10.1016/s0967-0637(03)00098-0

Tanoue, E., and Midorikawa, T. (1995). "Detection, characterization and dynamics of dissolved organic ligands in oceanic waters," in *Biogeochemical Processes and Ocean Flux in the Western Pacific*, eds H. Sakai, and Y. Nozaki, (Tokyo: Terra Scientific Publishing Company (TERRAPUB)), 201–224.

Tebo, B. M., Bargar, J. R., Clement, B. G., Dick, G. J., Murray, K. J., Parker, D., et al. (2004). BIOGENIC MANGANESE OXIDES: properties and mechanisms of formation. *Annu. Rev. Earth Planet. Sci.* 32, 287–328. doi: 10.1146/annurev.earth.32.101802.120213

Tebo, B. M., Nealson, K. H., Emerson, S., and Jacobs, L. (1984). Microbial mediation of Mn(II) and Co(II) precipitation at the O2/H2S interfaces in two anoxic fjords. *Limnol. Oceanogr.* 29, 1247–1258. doi: 10.4319/lo.1984.29.6.1247

Toyoda, K., and Tebo, B. M. (2016). Kinetics of Mn(II) oxidation by spores of the marine *Bacillus* sp. SG-1. *Geochim. Cosmochim. Acta* 189, 58–69. doi: 10.1016/j.gca.2016.05.036

van de Flierdt, T., Pahnke, K., Amakawa, H., Andersson, P., Basak, C., Coles, B., et al. (2012). GEOTRACES intercalibration of neodymium isotopes and rare earth element concentrations in seawater and suspended particles. Part 1: reproducibility of results for the international intercomparison. *Limnol. Oceanogr. Methods* 10, 234–251. doi: 10.4319/lom.2012.10.234

van Hulten, M. M. P., Middag, R., Dutay, J.-C., de Baar, H. J. W., Roy-Barman, M., Gehlen, M., et al. (2016). Manganese in the West Atlantic Ocean in context of the first global ocean circulation model of manganese. *Biogeosciences* 14, 1123–1152. doi: 10.5194/bg-14-1123-2017

Vedamati, J., Chan, C., and Moffett, J. W. (2015). Distribution of dissolved manganese in the Peruvian upwelling and oxygen minimum zone. *Geochim. Cosmochim. Acta* 156, 222–240. doi: 10.1016/J.GCA.2014.10.026

Vu, H. T. D., and Sohrin, Y. (2013). Diverse stoichiometry of dissolved trace metals in the Indian Ocean. *Sci. Rep.* 3:1745. doi: 10.1038/srep01745

Westerlund, S. F. G., Anderson, L. G., Hall, P. O. J., Iverfeldt, Å, Van Der Loeff, M. M. R., and Sundby, B. (1986). Benthic fluxes of cadmium, copper, nickel, zinc and lead in the coastal environment. *Geochim. Cosmochim. Acta* 50, 1289–1296. doi: 10.1016/0016-7037(86)90412-6

Wu, J., Roshan, S., and Chen, G. (2014). The distribution of dissolved manganese in the tropical–subtropical North Atlantic during US GEOTRACES 2010 and 2011 cruises. *Mar. Chem.* 166, 9–24. doi: 10.1016/j.marchem.2014.08.007

Yasuda, I. (2004). North Pacific intermediate water: progress in SAGE (Subarctic Gyre Experiment) and related projects. *J. Oceanogr.* 60, 385–395. doi: 10.1023/B:JOCE.0000038344.25081.42

Yasuda, I., Kouketsu, S., Katsumata, K., Ohiwa, M., Kawasaki, Y., and Kusaka, A. (2002). Influence of Okhotsk Sea Intermediate Water on the Oyashio and North Pacific Intermediate Water. *J. Geophys. Res.* 107:3237. doi: 10.1029/2001JC001037

Yiğiterhan, O., Murray, J. W., and Tuğrul, S. (2011). Trace metal composition of suspended particulate matter in the water column of the Black Sea. *Mar. Chem.* 126, 207–228. doi: 10.1016/j.marchem.2011.05.006

You, Y. (2003a). Implications of cabbeling on the formation and transformation mechanism of North Pacific Intermediate Water. *J. Geophys. Res.* 108:3134.

You, Y. (2003b). The pathway and circulation of North Pacific intermediate water. *Geophys. Res. Lett.* 30:2291. doi: 10.1038/nature09288

You, Y. (2005). Unveiling the mystery of North Pacific intermediate water formation. *Eos Trans. Am. Geophys. Union* 86:65. doi: 10.1029/2005EO070002

Zhang, J., and Nozaki, Y. (1998). Behavior of rare earth elements in seawater at the ocean margin: a study along the slopes of the Sagami and Nankai troughs near Japan. *Geochim. Cosmochim. Acta* 62, 1307–1317. doi: 10.1016/S0016-7037(98)00073-8

Zheng, L., Minami, T., Konagaya, W., Chan, C.-Y., Tsujisaka, M., Takano, S., et al. (2019). Distinct basin-scale-distributions of aluminum, manganese, cobalt, and lead in the North Pacific Ocean. *Geochim. Cosmochim. Acta* 254, 102–121. doi: 10.1016/j.gca.2019.03.038

Zheng, X.-Y., Plancherel, Y., Saito, M. A., Scott, P. M., and Henderson, G. M. (2016). Rare earth elements (REEs) in the tropical South Atlantic and quantitative deconvolution of their non-conservative behavior. *Geochim. Cosmochim. Acta* 177, 217–237. doi: 10.1016/j.gca.2016.01.018

Zurbrick, C. M., Gallon, C., and Flegal, A. R. (2017). Historic and Industrial Lead within the Northwest Pacific Ocean evidenced by lead isotopes in Seawater. *Environ. Sci. Technol.* 51, 1203–1212. doi: 10.1021/acs.est.6b04666

Conflict of Interest: The authors declare that the research was conducted in the absence of any commercial or financial relationships that could be construed as a potential conflict of interest.